NTNU

Norwegian University of
Science and Technology

Detection of Stiction in Control Valves

an Algorithm for the Offshore Oil and Gas Industry

Asgeir Kvam

Master of Science in Engineering Cybernetics

Submission date: June 2009

Supervisor: Ole Morten Aamo, ITK

Co-supervisor: Tu Duc Nguyen, Siemens Oil & Gas Offshore AS

Norwegian University of Science and Technology
Department of Engineering Cybernetics

Problem Description

The thesis is related to offshore oil and gas production. It builds upon the literature survey on CPM from A. Kvams project work fall 2008. The candidate should develop an algorithm that detects stiction in control valves and apply it to one or several cases from offshore oil and gas industry.

The problem description is divided in four parts:

1.
Study the offshore production plant model developed by T. Grong and Ø. Kylling summer/fall 2008. How does stiction in control valves affect the behaviour of the model? The candidate is free to establish a model on his own, but this is not recommended. Modifications can be done in order to produce a specified behaviour.

2.
Choose one or more methods for detection of stiction in control valves from the literature and apply the methods on the case.

3.
Based on experience from the project work and part 2, suggest new concepts for detection of stiction in control valves.

4.
Consider the possibility of applying the methods from literature and the suggested concepts on real offshore oil and gas data.

Assignment given: 09. January 2009
Supervisor: Ole Morten Aamo, ITK

Preface

This thesis is the result of the work in the 10th and final semester of the Master of Technology program at the Department of Engineering Cybernetics at the Norwegian University of Science and Technology (NTNU). The thesis has been performed during the spring semester of 2009.

I would like to thank my supervisors Professor Ole Morten Aamo at NTNU and Dr. Tu Doc Nguyen at Siemens Oil and Gas for guidance and feedback during the work. I would also thank Professor Morten Hovd for valuable mail correspondence.

I am thankful to my co-students at the office who have given me support and help during periods of little progress. Big thanks to Anne Baukol Risheim for proofreading.

Finally, I would thank my fiancée for all support and back up throughout this semester.

Trondheim, June 4, 2009

Asgeir Kvam

Abstract

Valve stiction is one of the largest stand-alone reasons for oscillatory behavior in process industry. It is reported by Siemens Oil and Gas that valve stiction is a problem that is hard and time consuming to detect at offshore production plants for oil and gas.

As a result, Siemens Oil and Gas wants to develop an algorithm that detects stiction. The algorithm is thought to be a feature of the logging system of Siemens in the future.

To better understand the problem and scope of stiction at a offshore oil and gas production plant, the effects of stiction is studied on a model of such a plant. The study shows that oscillations from stiction in the control valves of a first stage separator easily spread to downstream components such as the connected gas compressor.

An algorithm that detects stiction from routine operating data is developed in this thesis. The method in base for the algorithm is chosen from a variety of methods for stiction detection. To choose a suitable method in base for the algorithm a brief survey of methods for detecting stiction is given.

The algorithm output is a stiction index that indicate the presence of stiction in the data analyzed. The algorithm detects stiction in data from non-integrating processes with constant inputs and can be applied on data with a varying sample rate. Proper testing on real data from an offshore production plant remains to be done. The algorithm should also be improved to handle data containing noise.

Two new ideas of detecting stiction in integrating processes are presented in the end of the thesis. The new ideas try to regain the hidden ellipses in the PV-OP plots from data with stiction from integrating processes. The first idea is to plot the OP data against time shifted PV data, while the second idea is to plot the OP data against high-pass filtered PV data. Both the ideas show promising results but need to be further developed and tested before they can be applied in a future application for stiction detection.

Contents

List of Figures

List of Tables

Nomenclature

Ψ	Compressor characteristic equation
ρ_{metL}	Methane density, liquid phase
ρ_{oilL}	Oil density, liquid phase
A_c	Compressor duct area
A_{sep}	Separator area
C_4	Separator tuning parameter
C_v	Valve constant
c_{01}	Gas sonic speed
F_a	Valve actuator force
F_c	Valve Coulomb friction
F_f	Valve friction force
F_r	Valve spring force
F_s	Valve static friction
F_v	Valve viscous friction
F_{in}	Inlet molecular flow
F_{outG}	Outlet gas molecular flow
F_{outL}	Outlet oil molecular flow
F_{sep}	Separator boiling flow rate
L_c	Compressor duct length
m_c	Compressor mass flow
M_v	Valve stem mass

m_v	Valve mass flow
m_{in}	Inlet compressor mass flow
m_{out}	Outlet compressor mass flow
m_{rv}	Compressor recycle valve mass flow
n_c	Compressor shaft speed
N_{metG}	Number of methane moles in gas phase
N_{metL}	Number of methane moles in liquid phase
N_{oilL}	Number of oil moles in liquid phase
p_1	Valve upstream flow pressure
p_2	Valve downstream flow pressure
p_{ev}	Separator process equilibrium pressure
p_{in}	Inlet compressor pressure
p_{metV}	Methane vapor pressure
p_{out}	Outlet compressor pressure
p_{sep}	Separator pressure
R	Ideal gas constant
T_c	Compressor gas temperature
T_{sep}	Separator gas temperature
u_v	Valve opening
v	Valve stem velocity
V_{in}	Inlet compressor plenum
V_{oilL}	Oil volume, liquid phase
V_{out}	Outlet compressor plenum
V_{sep}	Separator volume
W_{met}	Methane mole weight
W_{oil}	Oil mole weight
x	Valve stem position

Z_{metI} Inlet molar methane fraction

Z_{metL} Mole methane fraction in liquid phase

Z_{oilI} Inlet molar oil fraction

Z_{oilO} Outlet molar oil fraction

Abbreviations

CC	Cross-Correlation
FDI	Fault Detection & Identification
NLA	Nonlinear Analysis
NTNU	Norwegian University of Science and Technology
MV	Valve Output
OP	Controller Output
PDF	Power density Function
PI	Proportional integral
PV	Process Variable
TSA	Time Shape Analysis

Chapter 1

Background

1.1 Introduction

Siemens delivers control and logging systems for offshore production plants. Such plants consist of several thousand valves and controller loops. An internal operation report from such a plant written by [Torpe and Dessen] have discovered that that there are many valves with stiction problems that cause poor and unwanted process behavior.

The operation report is not unique. Despite the fact that control theory has been an active research area for over 60 years, [Jelali, 2006], and [Desborough and Miller, 2002], state that 60% of all industrial controllers have performance problems.

One of the main causes for the poor control performance reported is oscillatory behavior, according to [Choudhury et al., 2005] and references therein. Oscillations in critical variables at a typical offshore oil and gas production plant lowers product quality, safety and economic margins and is unwanted. [Choudhury et al., 2005] also report that 30% of the oscillatory behaviour is present due to control valve problems.

Control valve problems occur from non-deterministic nonlinear dynamics inside the control valve. [Choudhury et al., 2005] concludes that *"among the nonlinearities in control valves, stiction is the most common and one of the long-standing problems in the process industry."*

In the mentioned operation report, a control valve was reported to have stiction problems for 3-4 years before the stiction problem was detected. The only way to confirm the stiction was by visual inspection of the valve stem during operation. The only way of fixing a worn-out valve, is to replace it during process service shutdown. A shutdown results in no production and production loss during startup period. Early detection of stiction in a valve can make service shutdown more efficient, by replacing both worn-out and soon to be worn-out valves. This can increase the time period between service shutdowns, saving time and money.

Siemens initially wanted to develop an algorithm that automatically detected and investigated poor control performance. [Kvam, 2008] presented a literature survey on Control Performance Monitoring and and suggested the Harris Index as a simple measure for evaluating control performance. Results showed that the Harris Index was hard to apply to real data the logging system of Siemens due to extensively data compression.

Because of this and the reported problems from valve stiction, Siemens rather wants a simple algorithm that detects stiction. The algorithm must applicable to all the different control loops in a typical oil and gas production plant. The algorithm is required to have a low computational burden since the it should be implementable online.

Siemens also wants to investigate how valve stiction in one component of a oil and gas production plant affects downstream components under different operating conditions such as inlet slug flow. Oscillations in one part of a plant will result in larger control action in control valves close to the source of oscillation, and the oscillations may easily spread. Larger control action results in increased wear and tear on the control valve.

To simulate different scenarios, a model of a typical oil and gas production plant should be used. Development and testing of a stiction detection algorithm is also more easily done on data from a known model. [Kylling, 2008] have developed a complete model of a production line from an offshore oil and gas platform. His model is used for simulation in this thesis. If not specified, the model of [Kylling, 2008] from now on should be read as the *production plant model*.

Some necessary background information is now given followed by a scope and emphasis of this thesis.

1.2 A production plant

A typical offshore production plant for oil and gas is given on figure 1.1. Crude oil from the well is separated into oil, water and gas. This is done offshore to simplify further transport. The crude oil can contain slugs of sand and large gas pockets making its composition unknown and not suitable for transport.

From figure 1.1 it can be seen that separation is done in three separators, each reducing pressure in the processed crude oil. The output pressure in the oil from separator S3 is near the atmospheric pressure. After separation, the gas is compressed for transport which require a high gas pressure. The later the gas is separated from the crude oil, the more the gas must be compressed, motivating for the compressor train structure, compressing the gas in several stages/compressors.

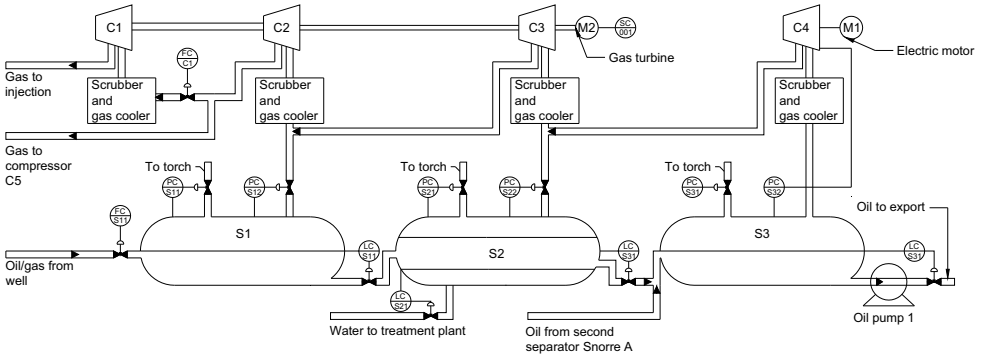

Figure 1.1: Overview of a production plant for oil and gas, from [Kylling, 2008]

1.3 Slug flow

Slug flow is a known problem at offshore production plants for oil and gas and can be described as periodic bubbles of gas inside bulks of multiphase liquid flow, according to [Storkaas et al., 2003]. Slug flow is divided into horizontal and gravity induced slugs.

Horizontal induced slug flow appears in horizontal pipelines, while gravity induced slug flow appear in a low point of pipeline, for instance at the bottom of a riser. Because of gravity, liquid accumulates in such a low point which blocks any gas transport. From a upstream pressure buildup and release of gas bubbles from the liquid, periodic oscillations in pipe pressure and mass are created.

The time period of the slugs are long, approximately 10 minutes and result in a variation in pipe pressure of pressure $5 - 6$ bars.

The oscillations in the pipe flow pressure and flow creates an unwanted disturbance to the first stage separator in a production plant. It also affects downstream components.

1.4 Control valve

Control valves are a crucial part of a process control systems. Each loop in a process control system has a process variable such as temperature, pressure, level etc. A controller is designed to keep the process variable at a desired value unaffected of internal or external disturbances. [Fisher, 2005] defines the control valve as the final control element that implements the controller strategy into the real process by manipulating flowing fluid.

To get a better understanding of how a control valve works, some necessary definitions of the notation used in association with the control valve followed by a description of the structure and the nonlinearities of a common control valve.

1.4.1 Notation

A precise notation is important when describing a control valve. In literature, there are many phrases used together in a vague mix such as, controller output, valve input, measured variable, controlled variable and manipulated variable.

The notation presented is widely used in industry and will be used throughout this thesis. The notation is illustrated in a general control structure in figure 1.2. OP is the controller output and a set point for the valve opening. MV is the valve output or valve stem position and describes the actual valve opening. Both MV and OP are always in the range from 0 to 1, where 1 denotes a fully opened valve and 0 denotes a closed valve. The last variable defined is the controlled variable or process variable PV, which is a measurement of the controlled medium.

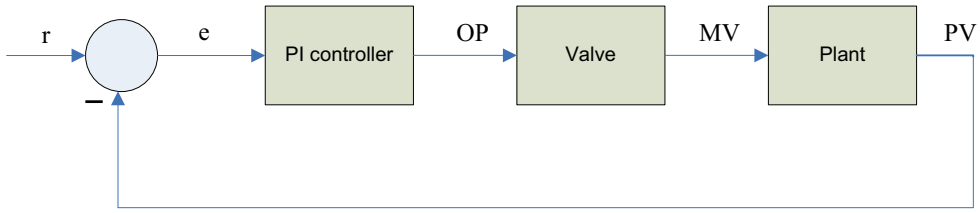

Figure 1.2: General process control structure

1.4.2 Assembly

Figure 1.3 shows the structure of a common pneumatic control valve since pneumatic valves are widely used in industry. The balance between the elastic force, air pressure and friction determine the position of the valve stem and flow rate through the valve. The valve is closed by the elastic force and opened by air pressure.

1.4.3 Friction

The force that is hard to determine and control in a valve is friction. Friction opposes any stem movement as defined by [Fisher, 2005] as: *A force that tends to oppose the relative motion between tho surfaces that are in contact with each other.* Two types of friction exist, static and dynamic friction. Static friction is the force that must be exceeded before any motion between two surfaces can occur. Dynamic friction is the friction force present when there is relative motion, acting in the opposite direction of motion.

From friction forces in mechanical valve assembly, several valve nonlinearities occur.

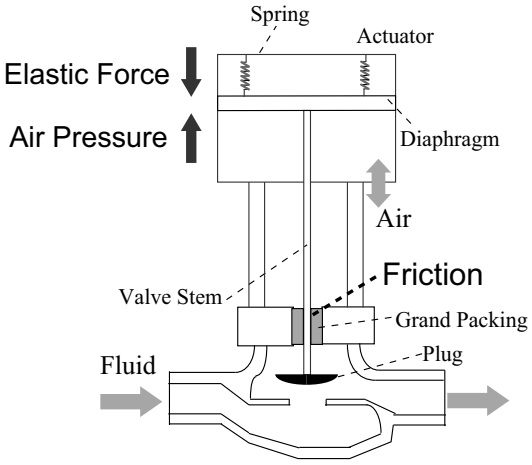

Figure 1.3: Structure of pneumatic control valve , from [Kano et al., 2004]

1.4.4 Nonlinearities

Friction forces create different nonlinearities in valve stem dynamics such as backlash, hysteresis, dead band, dead zone and stiction. As a result, OP and MV are not always the same. Different valves have different characteristics depending on size, valve type, operational conditions etc. A MV-OP plot is used to describe valve characteristics as in figure 1.4, and a MV-OP plot is mostly part of the valve data sheet.

[Choudhury et al., 2005] and references therein defines four valve nonlinearities as (with an illustration, see figure 1.4):

- Backlash: *"A relative movement between interacting mechanical parts, resulting from looseness, when the motion is reversed."*

- Hysteresis: *"Property evidenced by the dependence of the value of the output, for a given excursion of the input, upon the history of prior excursions and the direction of the current traverse"*, see figure 1.4 (a) and (c).

- Dead band: *"The range through which an input signal may be varied, upon reversal of direction, without initiating an observable change in the output signal"*, see figure 1.4 (b).

- Dead zone: *"A predetermined range of input through which the output remains unchanged, irrespective of the direction of change of the input signal"*, see figure 1.4 (d).

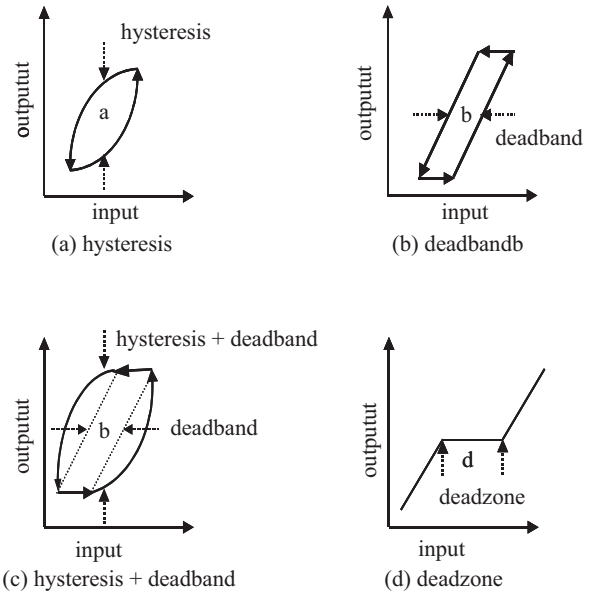

Figure 1.4: Valve nonlinearities, from [Choudhury et al., 2005]

1.5 Stiction

Stiction is defined by [Choudhury et al., 2005] as *"A property of an element such that its smooth movement in response to a varying input is preceded by a sudden abrupt jump called the slip-jump"* and is as described in the introduction a major problem in process industry.

Stiction is the only nonlinearity that introduces limit cycles[1]. Pure dead band and backlash can only introduce limit cycles in a integrating loop under feedback control.

The size of the stiction is the force necessary to move the valve stem out of a stuck position. In industry, stiction is measured in percent of the controller output necessary to move the valve stem.

When a valve stem is stuck in a closed loop controlled by a PI controller, the lack of change in the controlled variable result in an increased output from the controller due to the integral action in the controller. The controller output increases until the valve stem starts to move. The force necessary to keep the valve stem in movement is less than the force needed to move the stem. As a result the controlled variable starts to oscillate.

Because the valve stem sticks and slips the MV output has the form of a square pulse when stiction is present. In non-integrating processes this pulse is smoothened out by process dynamics, and the oscillations in the PV data

[1]A limit cycle is an isolated periodic orbit in the phase portrait and indicates that the system oscillates, [Khalil, 2002]

takes the form of an exponential rice and decay. For integrating processes, the squared pulse is integrated by the process and a triangular shaped oscillation occurs in the PV data.

1.6 Scope of thesis

The rest of the thesis is organized as follows:

- **Chapter 2** gives a survey of published methods that automatically detects stiction from routine operating data.
- **Chapter 3** presents the production plant model used to investigate the effects of stiction in a offshore production plant for oil and gas.
- **Chapter 4** contains a description of the valve model with stiction added to the production plant model to create stiction effects.
- In **Chapter 5**, the results from simulation of the production plant model is presented.
- In **Chapter 6**, an algorithm that detects stiction is presented and tested.
- **Chapter 7** presents two new ideas for detection of stiction.

Chapter 2

Review of methods for stiction detection

This chapter gives a review of different methods that detect stiction in a control valve. An overview of research in this area is necessary to suggest and assess methods that can be used in an algorithm that detects stiction. Initially, the chapter sets stiction detection in a larger context, before some methods are presented in three different parts depending on what type of analysis the methods are based upon. The chapter ends with an summarizing comparison of the presented methods.

2.1 History

Automatic detection of stiction is a fairly new research area that branches from Control Performance Monitoring (CPM). CPM was initiated by [Harris, 1989] in 1989 and during the 1990s many new methods for CPM was developed. Most of the CPM methods at that time did not diagnose the reason for poor controller performance, they only assessed whether performance was good or poor.

In the late 1990s, [Thornhill and Hägglund, 1997] presented some operational signatures that indicate the cause of an oscillation. Later, many methods for detecting valve stiction have been proposed, and some of these methods have been applied in the process industry. The methods vary in complexity and computational burden, and they have all some limiting assumptions for a general application.

Until recently, articles have been the only source of literature in the area of detecting stiction. The little established literature found are two books in the Springer Book Series *Advances in Industrial Control*: *Process Control Performance Assessment*, [Ordys et al., 2007], and *Diagnosis of Process Nonlinearities and Valve Stiction*, [Choudhury et al., 2008]. Because several authors have contributed with chapters in the second book, the chapters in

Table 2.1: Outline of methods for stiction detection

#	Principle	Reference
i.	Cross correlation	[Horch, 1999]
ii.	Derivative of PV data	[Horch, 2000]
iii.	Half period integral ratio	[Singhal et al, 2005]
iv.	Shapes in PV data using QSA[a]	[Rengasw. et al, 2001]
v.	Parallelogram in MV-OP plot	[Kano et al, 2004]
vi.	Shapes in PV data using finite derivatives	[Yamashita, 2006]
vii.	Fit PV data to stiction shapes	[Rossi and Scali, 2004]
viii.	Fit output if first integrator to triangular	[He et al, 2007]
ix.	Compute NLI and NGI[b], quantify using PV-OP	[Choud. et al, 2005]
x.	Predictability of a time trend and its surrogate	[Thornhill, 2005]
xi.	Multi-model estimation and detection of change	[Stenman et al, 2003]
xii.	Change (or lack of change) in OP and PV	[Yamashita, 2006]

[a]Qualitative Shape Analysis
[b]Non-Linear and Non-Gaussian Index

this book are referred in specific to tribute the correct authors.

[Horch, 2007] has tested a variety of methods on different data sets and assesses each method against each other. Horch presents the different methods and their performance in a short and well-arranged way by defining three different classes of stiction detection methods: *time shape analysis (TSA)*, *nonlinearity analysis (NLA)* and *fault detection & identification analysis (FDI)*.

Before the methods are described, an outline of methods with key references and principles are presented, see table 2.1. The methods are numbered from *i-xii*, where methods numbered i-vii belongs to the TSA class, methods numbered viii-ix belongs to the NLA class and methods numbered x-xii is from the FDI class.

2.2 Time domain shape analysis

Time domain shape analysis is a class of visual based methods. A known stiction pattern is recognized on either raw or processed valve data such as OP, MV or PV data. Early methods were only graphical, an operator needed to recognize the patterns visually, while the newest methods make use of mathematical fitting to known shapes that characterize the valve stiction.

i. One of the first attempts to automatically detect stiction was made by [Horch, 1999]. He uses the cross correlation (CC) between OP and PV data to indicate stiction. He observes that stiction introduces a phase lag of 90° (odd CC-function), while an aggressive controller or external disturbance introduces

a 180° phase lag (even CC-function). If the CC-function is between an odd an even form, no conclusions can be made.

The method applies to non integrating processes controlled by a PI controller. To ensure the quality of the indications made, an oscillation must be detected before the CC-function is calculated.

ii. [Horch, 2000] later developed another principle that is applicable on integrating processes. They compute the probability density function (PDF) of the second derivative of the PV signals to detect stiction.

Integrating processes with stiction produce a PV signal with a triangular pulse. The second derivative of a triangular pulse is single peaks in an ideal case. For self-regulating processes[1] the PDF of the first derivative is used. The following description applies to both integrating and non-integrating processes and the derivative should be read as both first and second derivative dependent on what process that is analyzed.

In a non-ideal case, noise will be present and the PV signal must be filtered before it is differentiated. The filter cut-off frequency is three times the oscillation frequency.

If the PDF of the derivative can be fitted to a Gassian distribution (peak around zero frequency), stiction is present. If the PDF fits a "camel"-formed distribution (two peaks), it is likely that there is a sinusoidal oscillation, since a pure sinus signal have two peaks in its signal spectrum. See figure 2.1 for an example of second derivatives with histograms for a stiction and non-stiction case.

The method requires only PV-data, but needs to know whether the process is an integrating process or not.

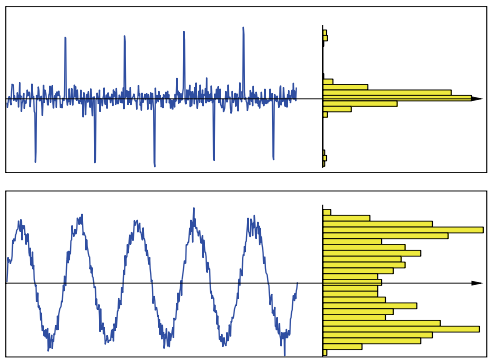

Figure 2.1: Second derivatives of PV with histograms for a stiction (top figure) and non-stiction case (bottom figure), from [Horch, 2000]

[1] A process with its poles in the right half plane. Integrating processes has at least one pole at the imaginary axis and are thus *not* a self-regulating process.

iii. [Singhal and Salsbury, 2005] propose a simple method for detection of valve stiction. Their main principle is to recognize two shapes in the control error signal, an exponential rice and decay and a sinusoidal wave. If valve stiction is present, the control error signal is similar to a exponential rise and decay due to a pulse in the OP data. The pulse in the OP data is a known phenomena when stiction is present in self-regulating plants. A sinusoidal wave arises from aggressive control, for instance an under damped mass-spring system.

To distinguish between the two shapes, an index is computed from the half period integrals of a single oscillation. The index is defined as:

$$R = \frac{A_1}{A_2} \tag{2.1}$$

where A_1 is the integral area of the half period before the peak and A_2 is the integral area of the half period after the peak. See figure 2.2 for an illustration of the different control error signal shapes and the different integrals.

Based on the value of R for the two shapes described, [Singhal and Salsbury, 2005] define a decision rule:

$$\begin{aligned} R > 1 \quad &\Rightarrow \quad \text{valve stiction} \\ R \approx 1 \quad &\Rightarrow \quad \text{aggressive control} \end{aligned}$$

To avoid that wrong conclusions are made, [Singhal and Salsbury, 2005] assume that the controller output is not saturated[2], the oscillations are not from an external disturbance and the process analyzed is not an integrating process. The PV data of a purely integrating processes often take a triangular shape where the two integrals A_1 and A_2 are equal in the presence of stiction.

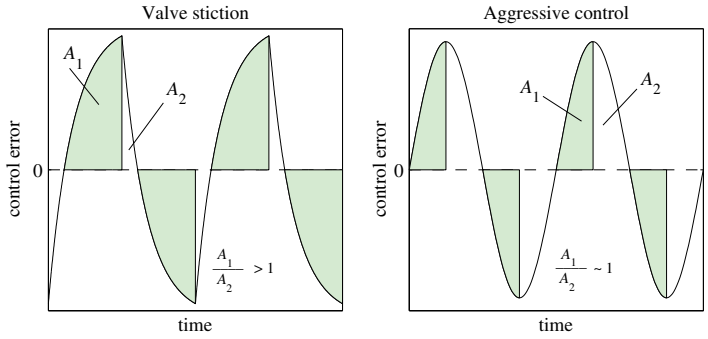

Figure 2.2: Control error signal shapes for stiction and aggressive control, from [Singhal and Salsbury, 2005]

[2]Saturation may introduce oscillations in a control loop

iv. [Rengaswamy et al., 2001] use a qualitative shape analysis (QSA) to detect shapes in process time data that characterize stiction. In short, the QSA breaks down and represent the time data from a set of pre-defined primitive shapes. By defining stiction as a specific sequence of some primitives (for instance triangular or square shapes), stiction is present if such a sequence is identified.

The fundamental part of the QSA is to identify the primitives. The identification is done using neural networks. [Rengaswamy et al., 2001] defines neural networks as *"computing systems composed of highly interconnected layers of simple neuron-like processing elements, which process information by their dynamic response to external inputs."*

In order to work satisfactory, the neural network must be trained to detect at least an increasing and decreasing trend. To isolate such a trend, a time window containing the trend must be specified which limits the adaptivity and generality of the method. The complex identification increases the computation time.

v. [Kano et al., 2004] exploit the form of the MV-OP plot to detect stiction. With stiction, the MV-OP plot is a parallelogram shown in figure 4.1. The parallelogram changes size from a change in stri-band and slip-jump vectors. Stiction is detected by detecting the parallelogram and its size in a recursive function:

$$F(t) = max\{min\{F(t-1) + \Delta u(t), F_{max}\}, 0\} \tag{2.2}$$

where $u(t)$ is the controller output. To obtain F_{max} and an initial value $F(0)$, an optimization problem must be solved which complicates the method. The results from the method are only reliable when there is a strong correlation between $u - F$ and y, which limits the usage of the method. Despite these limitations, [Kano et al., 2004] were one of the first to try to quantify the degree of stiction.

vi. The method of [Yamashita, 2006] is similar to the method of [Rengaswamy et al., 2001]. [Yamashita, 2006] defines three qualitative primitives: increasing (I), steady (S) and decreasing (D). Combining the primitives, nine fragments are defined in an MV-OP-plane to represent a type of movement. Four of these fragments are typical for valve stiction, see figure 2.3.

The identification of the fragments is based on the time derivatives of the OP and MV data. If noise is present, the identification is done by use of the finite differences compared to threshold values.

By counting the time period of IS and DS in these fragments, the degree of stiction can be estimated in an index:

$$\rho_2 = \frac{\tau_{ISII} + \tau_{ISSI} + \tau_{DSDD} + \tau_{DSSD} +}{\tau_{total} - \tau_{SS}} \tag{2.3}$$

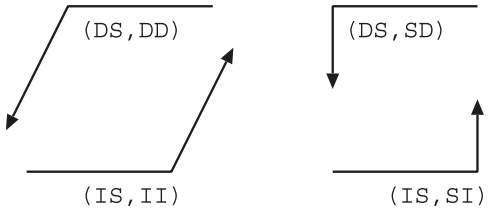

Figure 2.3: Combination of primitives typical for stiction, from [Yamashita, 2006]

where the subscripts denote the number of specific fragment samples in a data set. A index greater than 0.25 indicates valve stiction in the observed loop. A drawback for this method is that MV data must be available[3]. As for the method of [Rengaswamy et al., 2001], identification of the fragments is complex for data containing noise.

vii. [Rossi and Scali, 2004] use a first-order-plus-time-delay (FOPTD) process model with stiction to produce different oscillation shapes in the MV, OP and PV data that is compared to the real case data.

The different shapes are made by variation of three parameters: the controller gain K_c, the process time constant τ and the process time delay θ. From an analyze of the different oscillation shapes, three approximation curves are defined: a sinus wave (S), relay curve (R) and a triangular curve (T).

By variation of the parameters for the tree approximation curves, a fit to the real case data is made. For each fit, the mean square errors (E_S,E_R and E_T) between the fitted curve and the real case data are calculated. A stiction index is defined as

$$S_I = \frac{\bar{E}_S - \bar{E}_{RT}}{\bar{E}_S + \bar{E}_{RT}} \tag{2.4}$$

where $E_{RT} = min\{E_R, E_T\}$ and bars mean average value on all half cycles present in the real data. $S_I \in (-1, 1)$ where negative values indicate a better sinus approximation and positive values indicate a relay or a triangular approximation and stiction may be present. When the index is close to zero, the approximations are equal and the presence of stiction cannot be concluded.

When noise is present, the uncertainty of the index increases. There are no limitations on process type for this method, and only PV data are needed to apply the method.

viii. A very similar method to the method presented above is the method of [He et al., 2007]. Their principle is to fit the output of the first integrator after the valve in the control loop to either a triangular or sinusoidal wave. With

[3]MV data are usually not logged in industry according to [Choudhury et al., 2008].

valve stiction the valve output is a square pulse and integration of a square pulse is a triangular pulse.

For self-regulating loops, the data to fit is the OP data (since the controller has integral action), for an integrating loop the PV signal is the data to be fitted. After fitting the correct data to both triangular and sinusoidal wave, a stiction index is calculated in nearly the same way as the index of [Rossi and Scali, 2004].

In contrast to [Rossi and Scali, 2004], [He et al., 2007] demands some knowledge about the process in order to choose the correct data to be fitted.

2.3 Nonlinearity analysis

Nonlinearity analysis is a class of purely mathematical based methods that are designed to detect a nonlinearity in the valve. The methods result in a nonlinearity index that quantifies the size of the nonlinearity.

ix. One of the more complete methods for both detection and quantification of stiction was developed by [Choudhury et al., 2005]. They initially computed a nonlinearity and non-Gaussian index (NLI and NGI) using signal bicoherence, a normalization of the bispectrum[4] of a signal. It is assumed that the process is locally linear and that no nonlinear disturbances enter the loop assessed. Stiction is present if both the NGI and NLI measures are positive.

In the second step, the PV-OP plot is used to diagnose the stiction *after* a nonlinearity is detected. It is important to note that the data samples must be filtered prior to the diagnosis. The filter must be constructed such that the nonlinearity is not filtered away. Choudhury et al. [2005] suggest three different diagnosis strategies depending on the data available and its quality:

- If the loop contains a smart valve, MV data are present and can be plotted against PV data. The width of the cycling patterns in such a plot provides the amount of stiction. Smart valves are not yet to be used in most of the process industry.
- If the MV data are not available, an ellipse is fitted to the PV-OP plot. The maximum width is calculated from the fitted ellipse in the OP direction. The maximum width is the size of the stiction.
- If an ellipse cannot be fitted, a clustering technique is used to locate the mean of the PV. The mean of the ellipse is a narrow strip because most of the data points in an OP-PV plot are in the top and bottom of the ellipse. The width in the OP direction between the two narrowing MV strips gives the size of the stiction.

[4]The bispectrum is defined in [Choudhury et al., 2008] as *"the frequency domain representation of the third order cumulant or moment"*.

[Choudhury et al., 2005] used the PV-OP plots only to quantify the size of the stiction after a nonlinearity is detected. Some of the time domain shape analysis in section 2.2 use PV-OP plots to detect stiction and may detect false stiction when noise and external disturbances are present. Process dynamics can also hide the shapes in the PV-OP plots. The detection of a nonlinearity removes these false detections. The method of [Choudhury et al., 2005] is thus more general and accurate, but also more complex and heavy to compute than the time domain based methods.

x. [Thornhill, 2005] has developed a method for *finding the source of a nonlinearity in a process with plant-wide disturbance.* She and her references observe that the bispectrum in the method of [Choudhury et al., 2005] is zero for symmetrical waveforms such as triangular and square. This limits the performance of their method when such waveforms are present.

To counteract this drawback, [Thornhill, 2005] compared the predictability of a time trend against its surrogate[5]. Nonlinearities are more predictable than its surrogate time series. From a computation of the mean square prediction errors for the time and surrogate data (Γ_{test} and Γ_{surr}), a nonlinearity index is defined as

$$N_{Thorn} = \frac{\bar{\Gamma}_{surr} - \Gamma_{test}}{3\sigma_{\Gamma_{surr}}} \tag{2.5}$$

where $\bar{\Gamma}_{surr}$ is the mean of the surrogate prediction errors and $\sigma_{\Gamma_{surr}}$ is its standard deviation. Nonlinearity is present if $N_{Thorn} > 1$ and the highest index in a plant with a plant-wide nonlinearity is probably the source of the nonlinearity. The same principles for quantifying stiction as [Choudhury et al., 2005] thus can then be applied to gain more info about the nonlinearity.

The method uses only PV data, but the data require some preprocessing which increases the computational load.

2.4 Fault detection & identification analysis

The last class of methods is *Fault detection & identification analysis.* Fault detection in this context means to detect a change (or lack of change) in valve output (MV or PV) when OP is changed. The identification methods identifies a stiction parameter if stiction is present.

xi. [Stenman et al., 2003] purpose a method for stiction detection based on a multi-model estimation and a detection of a change. Their origin is a simple stiction model

[5]Surrogate data are data constructed from the same power spectrum as its time trend, but with a random phase added.

$$x(t) = \begin{cases} x(t-1), & \text{if } |u(t) - x(t-1)| \leq d \\ u(t), & \text{otherwise} \end{cases} \tag{2.6}$$

where x is valve output, u is controller output and d is the stiction friction force. From (2.6), a equation for stiction detection is derived

$$x(t) = (1 - \delta(t))x(t-1) + \delta(t)u(t) \tag{2.7}$$

where $\delta(t)$ is a binary mode parameter which is one if a jump in $x(t)$ occurs and zero otherwise. Assuming linear pipe dynamics, a process model with stiction is shown in figure 2.4

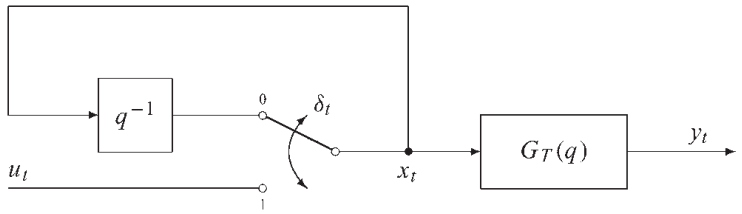

Figure 2.4: Data driven process model with stiction, from [Stenman et al., 2003]

By using segmentation from the literature of change detection, an estimate of the mode parameter $\delta^N = (\delta_1, ..., \delta_N)$ sequence is calculated. If jumps occur in the estimated sequence (δ_i), stiction is present. The amount of stiction is dependent of the number of jumps estimated. The method does not require any process information or that any oscillations are present and uses only PV data.

xii. Another method of [Kano et al., 2004] exploits the change (or lack of change) in the MV or PV data to detect stiction. If a valve is stuck, the MV or OP value is naturally constant. The difference in the valve output,

$$\Delta y(t) = y(t) - y(t-1) \tag{2.8}$$

is compared to a threshold value ϵ. If $|\Delta y| < \epsilon$, the difference between the maximum and minimum controller output $(\tilde{u})$ and the difference between the maximum and minimum valve position $(\tilde{y})$ is calculated. Further, thresholds for these differences are defined: ϵ_u for $\tilde{u}$ and ϵ_y for $\tilde{y}$.

When the controller output is above its threshold and the position difference is below its threshold $(\tilde{u} \geq \epsilon_u,\ \tilde{y} \leq \epsilon_y)$, stiction is concluded.

An index is suggested to be the ratio (ρ) of time samples with stiction to all the time samples. The index lies in the interval $\rho \in (0, 1)$, where values close to one indicates a high possibility for stiction and no stiction is present when the index is zero. The stiction can be quantified by taking the mean of $\tilde{u}$ when stiction occurs.

2.5 Comparison of methods

A comparison of the methods described in this chapter is presented in table 2.2. The table lists the key assumptions of the methods together with some pros and cons. The table also gives an estimate of the computational load of the methods. The table is inspired from the table of [Horch, 2007].

All the methods rely on different assumptions. The assumptions mainly consider the data available and the structure of the process analyzed. [Choudhury et al., 2008] states that only 5% of the valves in industry have MV data available. As a result, methods that use MV data have a relative limited usage in the industry.

The most important process knowledge needed is to know whether the process is an integrating process or not. Because of this, there are no methods that can be applied to all kinds of processes, and some process knowledge must exist to choose a proper method.

A majority of the methods require that oscillations are detected before they can be applied. Methods that detect oscillations are a solved problem, and some good methods are given in [Hägglund, 1995], [Thornhill and Hägglund, 1997] and [Salsbury and Singhal, 2005]. However, to apply such a method prior to apply a method for stiction detection increases the overall computational load.

In the TSA class, almost all methods have a low computational load. No heavy transformations are needed, the raw time measurements can be used directly. Depending of principle, the methods in this class are sensitive to noise. A derivation of a noisy signal results in an even more nosy signal, for instance. Filtering may help, but can destroy the nonlinear shapes of the signal characteristic for stiction.

The methods in the class of NLI detect a nonlinearity before the stiction is quantified. To detect a nonlinearity, the time domain data must be Fourier transformed, increasing the computation load. An advantage of the methods in this class is that they are purely mathematical and can detect a nonlinearity not visible for the human eye.

The methods from the last class detect a change or lack of change in the MV and OP data. This principle sounds simple and should require a low computational load. However, multi-model identification require a high computational load, see the method of [Stenman et al., 2003]. To set a threshold for each loop analyzed complicates the use of the other method in this class, the method of [Kano et al., 2004].

Table 2.2: Comparison of methods for stiction detection

	Load	**Assumptions**	**Pros (+)/ cons (−)**
i.	Low	⋆ OP and PV available ⋆ Non-int. process with PI ⋆ Oscillations detected ⋆ No compression	+ Simple, intuitive − Not for all loop types − Strong assumptions
ii.	Low	⋆ SP and PV available ⋆ Int. or non-int. process?	+ Simple + Signal shape not important − Rely on proper filtering
iii.	Low	⋆ PV and SP available ⋆ Non-int. process ⋆ Controller not saturated	+ Intuitive + Handles varying sample time − Sensitive to noise
iv.	High	⋆ OP and PV available ⋆ Some process knowledge ⋆ An isolated time trend	+ Flexible − Complex − Sensitive to noise
v.	Low	⋆ OP and MV available ⋆ Correlation ⋆ Opt. problem solved initially	+ Quantifies stiction − MV data required − Sensitive to noise
vi.	Medium	⋆ OP and MV available	+ Intuitive + Quantifies stiction − Complex when noise is present
vii.	Medium	⋆ PV available ⋆ Clear shape forms	+ Flexible + Reliable − Sensitive to noise
viii.	Medium	⋆ SP and OP or PV available ⋆ Int. or non-int process? ⋆ Oscillations detected	+ Flexible + Handles some noise − Complex fitting
ix.	High	⋆ OP and PV available ⋆ Locally linear process ⋆ No ext. nonl. disturbances	+ Quantifies stiction, reliable + Fails for tri. or square signals − Complex computation
x.	High	⋆ PV available ⋆ Oscillations detected	+ Flexible − Not stiction specific - Heavy computation
xi.	High	⋆ PV available ⋆ Multi-mode identification	+ Applies to non-oscillation data − Heavy computation
xii.	Medium	⋆ MV or PV available ⋆ Low process delay	+ Simple − Quantifies stiction − Threshold set for each loop

Chapter 3

Production plant model

The production plant model described in this chapter is a model made by [Kylling, 2008]. The model is a simplified version of the oil and gas production plant described in section 1.2. A summary of the most important aspects of the plant model derivation is given here. For a more detailed description, the reader is referred to Kyllings project report. An overview of the model is presented before each component is studied. The control structure of the model is given in the end of the chapter.

3.1 Process overview

The model of [Kylling, 2008] which is illustrated in figure 3.1 consists of two separators (S1 and S2) each connected to a scrubber and gas cooler, a gas turbine (M2) and two gas compressors (C2 and C3). The model input is crude oil from well and gas from compressor C4, the model output is oil to separator S3 and gas to compressor C1.

[Kylling, 2008] does these model simplifications to lower simulation time and to reduce the model complexity. Troubleshooting and implementation is thus easier. A model of each component in the production plant model is now presented followed by a description of the control structure of the model.

3.2 Separator

3.2.1 Function

The separator separates crude oil from well into gas and oil. In a real case, sand and water are also part of the crude oil, blended in a complex mix. [Kylling, 2008] models a two-phase separator that separates gas and oil, assuming that water is mixed and part of the the oil fraction. He further assumes that the gas contains of only methane (CH_4), and the oil only contains the component

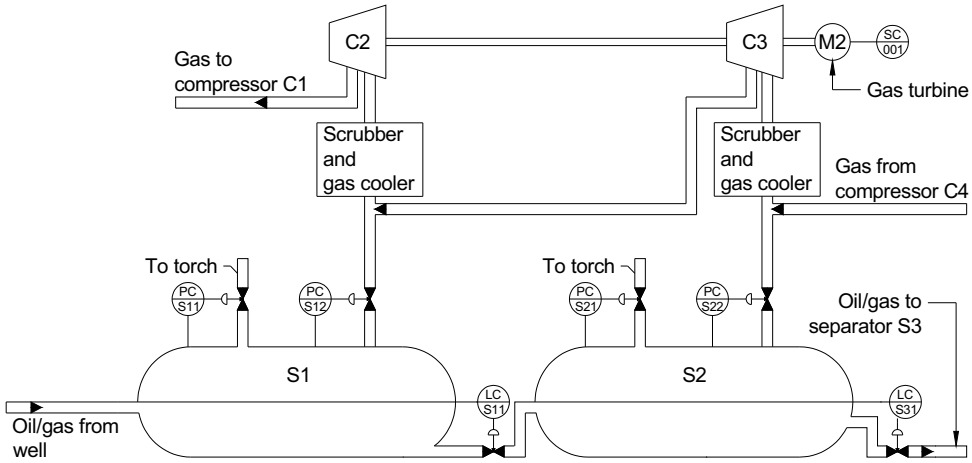

Figure 3.1: Overview of production plant model, from [Kylling, 2008]

hexane (C_6H_{14}). The final assumption is that the oil remain in a liquid phase, the oil can not vaporise.

The crude oil is then a blend of three components, methane in gas form (metG), methane in liquid form (metL) and hexane in liquid form (oilL). From now on, oil should be read as hexane.

3.2.2 Model

For each component, a mole balance is derived using a mole conservation law

$$\dot{N}_{oilL} = Z_{oilI}F_{in} - Z_{oilO}F_{outL} \tag{3.1}$$

$$\dot{N}_{metL} = Z_{metI}F_{in} - Z_{metL}F_{outL} - F_{sep} \tag{3.2}$$

$$\dot{N}_{metG} = F_{sep} - F_{outG} \tag{3.3}$$

where N_{oilL} is the number of hexane moles, N_{metL} is the number of methane moles in liquid phase, N_{metG} is the number of methane moles in gas phase. $Z_{oilI} = 1 - Z_{metI}$ is the molar oil fraction in the inlet molecular flow F_{in}, Z_{metI} is the molar methane fraction in the same flow. $Z_{oilO} = 1 - Z_{metL}$ is the molar oil fraction in the outlet liquid flow F_{outL}. $Z_{metL} = \frac{N_{metL}}{N_{oilL}+N_{metL}}$ is the molar methane fraction in liquid form inside the separator.

F_{sep} is the boiling flow rate of methane in liquid phase that vapors to methane in gas phase, and defined as

$$F_{sep} = C_4(p_{ev} - p_{sep}) = C_4(p_{metV}Z_{metL} - p_{sep}) \tag{3.4}$$

where p_{ev} is equilibrium[1] pressure, estimated using Rault's law. p_{sep} is the separator pressure, derived from the ideal gas law[2]. P_{metV} is the methane vapour pressure and Z_{metL} is still the molar lipquid methane fraction in the separator. C_4 is a tuning parameter, deciding how fast separator process converges to equilibrium.

In order to do level control, an expression for the liquid volume inside the separator V_{oil} is needed. The amount of moles in liquid form is is combined using basic physics to derive liquid volume

$$V_{oilL} = \frac{W_{oilL}N_{oilL}}{\rho_{oilL}} + \frac{W_{met}N_{metL}}{\rho_{metL}} \tag{3.5}$$

A constant known separator area A_{sep} is assumed for all levels and the level is easily computed from

$$h_{oil} = \frac{V_{oil}}{A_{sep}} \tag{3.6}$$

3.3 Scrubber and gas cooler model

Before the separated gas is compressed, it is cooled down. A gas with a low temperature has a higher molecule density than a gas with a high temperature, which makes the compressor more efficient. When a gas is cooled, droplets easily arise. To remove these droplets and other unwanted liquid from the separator gas flow, a scrubber is placed downstream to the gas cooler.

[Kylling, 2008] assumes that both the gas cooler and scrubber are ideal elements, behaving as described above without introducing extra dynamics in the production plant model. Since gas temperature is lowered, an extra pressure drop between the separator and compressor is added.

3.4 Compressor

3.4.1 Function

[Egeland and Gravdahl, 2003] described the function of a compressor, which is to compress the gas by increasing its pressure. This is done by an acceleration of the fluid followed by a deceleration of the same fluid. The acceleration is done by an impeller driven from a rotating shaft. A diffuser decelerates the fluid.

The acceleration increases the fluid kinetic energy which is converted into increased potential energy by a pressure rise in the fluid. These principles

[1] Equilibrium occurs when methane dissolved in the liquid no longer vapors to methane gas

[2] ($P_{sep}V_{metG} = p_{sep}(V_{sep} - V_{oilL} = N_{metG}RT_{sep})$

can be explained from Bernoulli's equation for frictionless incompressible flow along a streamline:

$$\frac{p_1}{\rho} + \frac{v_1^2}{2} + gz_1 = \frac{p_2}{\rho} + \frac{v_2^2}{2} + gz_2 \tag{3.7}$$

where p is pressure, ρ is the fluid density, v is the fluid velocity and gz is the potential energy. Left and right hand side is the total fluid energy before and after deceleration. Since the fluid does not have any horizontal movement ($z_1 = z_2$) before and after declaration, the decrease in kinetic energy ($\frac{C_1^2}{2}$) results in a increase in fluid pressure.

The compressor operation is limited by both high and low mass flow, according to [Egeland and Gravdahl, 2003]. At high mass flow, choking occurs when reaching the sonic speed in a compressor component. At low mass flow surge occurs when a drop in mass flow results in a decreased pressure, which again reduces the mass flow through the compressor.

Surge is characterized by large oscillations in the mass flow of the compressor, and the mass flow may even be reversed. Surge can in worst case destroy the compressor and components connected up- or downstream of the compressor and is thus unwanted. To prevent surge, a recycle vale can be installed around the compressor, ensuring a mass flow above the surge limit.

All compressors have their own compressor characteristics, describing the safe operation working points for different mass flows, fluid pressures and shaft speeds.

3.4.2 Model

The compressor type used in production plants for oil and gas is mainly a centrifugal compressor. Kyllings compressor model is a modified version of a centrifugal compressor model developed by [Egeland and Gravdahl, 2003]. The main model equations will be presented in this section. The reader is referred to chapter 13 in [Egeland and Gravdahl, 2003] for details about the model derivation.

The compressor model consists of a centrifugal compressor with a recycle valve to avoid surge, see figure 3.2. Using control volume considerations from fluid dynamics, two fixed plenums are defined: Inlet (V_{in}) and outlet (V_{out}) plenum.

To describe the dynamics of the compressor, mass and momentum balances are applied. The mass balance describes the pressure in the two plenum and the mass flow through the compressor. The mass balance describes the forces acting on the compressor shaft.

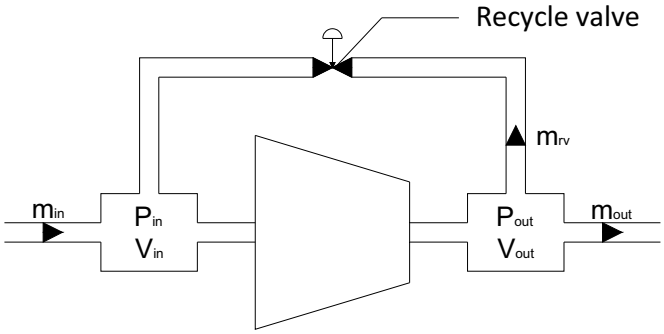

Figure 3.2: Compressor in- and outlet conditions, from [Kylling, 2008]

Assuming that the process is isentropic[3] and that methane is an ideal gas[4] the mass balance for the inlet plenum becomes

$$V_{in}\dot{\rho}_{in} = \frac{V_{in}}{c_{01}^2}\dot{p}_{in} = m_{in} + m_{rv} - m_c \tag{3.8}$$

where ρ_{in} is inlet density, p_{in} is inlet pressure, m_{in} is inlet mass flow, m_{rv} is mass flow through the recycle valve, m_c is the compressor mass flow , c_{01} is the sonic speed of gas, T_c is compressor temperature and γ is specific gas weight.

Similarly, the mass balance for the outlet plenum pressure is

$$V_{out}\dot{\rho}_{out} = \frac{V_{out}}{c_{01}^2}\dot{p}_{out} = m_{in} + m_{rv} - m_c \tag{3.9}$$

where ρ_{out} is outlet density, p_{out} is outlet pressure, m_{out} is outlet mass flow. To describe the mass flow through the compressor, the in- and outlet pressures are combined in a mass balance for the compressor

$$L_c\dot{m}_c = A_c(\Psi_c(n_c, m_c)(p_{in} - p_{out})) \tag{3.10}$$

where L_c is the length of the compressor duct, A_i is the area of the same duct. $\Psi(n_c, m_c)$ is the compressor characteristic extracted from compressor data sheet and polynomial approximations, giving a relation between compressor shaft speed n_c and compressor mass flow m_c.

The last model equation describes the different forces acting on the compressor shaft running the compressors. In the model of [Kylling, 2008] one gas turbine drives two compressors through one shaft. A torque balance for the shaft that drives the two compressors then becomes

[3]Egeland and Gravdahl, [Egeland and Gravdahl, 2003] defines isentropic processes as *" processes where there is no entropy production"*, meaning that there is no heat conduction and no internal viscous work.

[4]Ideal gas is a gas where the molecules are non-interacting, which is an common assumption at normal temperatures and pressures

$$I_{tot}\dot{\omega} = \tau_d - \tau_{c1}(N_{c1}, m_{c1}) - \tau_{c2}(N_{c2}, m_{c2}) \tag{3.11}$$

where I_{tot} is the total inertia of all rotating equipment acting on the shaft. [Kylling, 2008] suggest an estimate of this size based on compressor data and physical considerations. τ_d is the drive torque from the gas turbine. $\tau_{c1}(N_{c1}, m_{c1})$ and $\tau_{c2}(N_{c2}, m_{c2})$ is compressor torque for each compressor, extracted from compressor data and polynomial approximation. See [Kylling, 2008] for details.

3.5 Control structure

After all components in the production production plant model have been described, a brief overview of the control structure in the model is now given. The main controllers in the production production plant model are:

Table 3.1: Controllers of the production production plant model

Controller	Controller type	Symbolic name
Compressor anti surge	PI with nonlinear gain	ASCC21
Gas turbine speed	PI	SC001
Separator level	PI with anti-windup	LCS11
Separator pressure	PI with anti-windup	PCS11

The controller symbolic names are extracted from figure 3.1. The two first letters denote compressor type and the next two letters denote process component. The last letter is the controller number. For instance, PCS12 is pressure controller number two in separator one.

3.5.1 Anti-surge controller

The main purpose of the anti-surge controller is to keep the compressor from going into surge. This is achieved by using a recycle valve around the compressor. When pressure or mass flow drops, the recycle valve opens and compressed gas are sent back into the compressor to maintain a minimum mass flow.

The anti-surge controller used in Kyllings production plant model is a simplified version of a real anti-surge controller used in industry. Some safety functions are removed, but the core control structure is kept. All controller parameters are from a real anti-surge controller making the model very realistic.

The set point for the anti-surge controller is computed from measurements of compressor mass flow and pressure. A non-linear gain is added to the

increase the controller gain when approaching the surge-line[5]. A damping like functionality is also added to the controller gain to increase controller action if the mass flow or pressure gradients reaches a given limit.

3.5.2 Gas turbine speed controller

The two compressors C2 and C3 are driven by a common shaft. The shaft is driven by a gas turbine, where the shaft speed is controlled by a cascaded PI controller. The main objective of the speed controller is of course to maintain the shaft speed regardless of the different loads on the two compressors connected to the shaft.

Another important issue is to minimize the pressure loss from the separators to the compressors. Any pressure drop in the separators must be retrieved in the compressors, specially in the low pressure separator S2. Therefore, the valve at gas outflow from S2 is desired to be almost open.

These two objectives justify the need for two controllers in cascade where the first controller calculates the shaft speed set point based on measured and desired valve opening. The second controller puts out torque to the gas turbine from deviation in measured and desired shaft speed. The cascade controller is illustrated in figure 3.3.

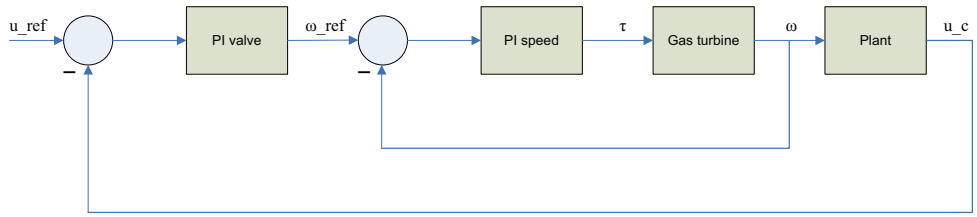

Figure 3.3: Structure of gas turbine speed controller

3.5.3 Separator level controller

In addition to separate inlet well flow into oil and methane, the separators also act as buffer tanks to ensure a more steady outlet product stream from the process plant. As a result, the separator level controllers are not tightly tuned. [Kylling, 2008] uses a volume controller in his production plant model, where the set point is half of the separator volume.

[5]The surge-line is a line in the compressor characteristics that defines the limit for safe operation of the compressor. If the surge.line is crossed it is very likely that the compressor will go into surge.

3.5.4 Separator pressure controller

Pressure control is necessary to keep the pressure in the separators within safe values. High pressure peaks can destroy the separator process, mixing already separated methane into the oil. Some pressure must be obtained in the separators, to save energy in the compressors. If, for instance the crude oil looses all its pressure in separator S1, compressor C3 cannot compress the gas satisfactory.

In addition to standard pressure control, [Kylling, 2008] models a safety pressure controller for the separators. The controller ensures that pressure peaks from inlet flow do not reach downstream process components. Because the peaks must be counteracted immediately, it is assumed that the safety pressure controller output is unlimited and without any valve dynamics. The amount of gas that exceeds the safety pressure limit is led to a flare that burns the gas.

Chapter 4

Valve model with stiction

This chapter presents a valve model with stiction. Prior to the presentation of the valve model, a more detailed description of stiction is given.

4.1 Stiction characteristics

To gain a better understanding of stiction, a more visual description is now given. The discription is based on the MV-OP plot in figure 4.1.

When a valve is at rest (A in figure 4.1), the controller output must be increased to overcome the dead band and stiction force. After overcoming the stiction force, the stem slips (C-D). If the controller require more stem movement, the stem moves until the valve sticks again, (E). When in movement, dynamic friction is present, which can be lower than the static friction, see figure 4.2. When the controller output closes the valve, the valve behaves equal in the opposite direction (E-F-G-A).

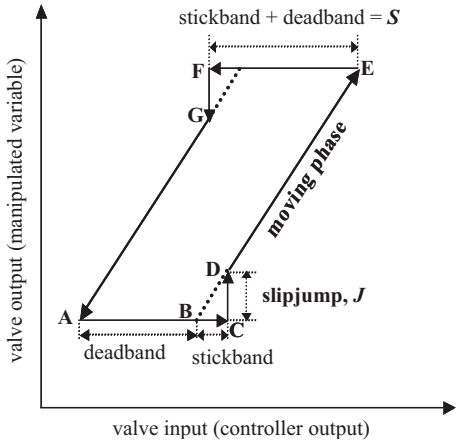

Figure 4.1: MV-OP plot characteristic for stiction, from [Choudhury et al., 2005]

It is important to notice that dead band only occurs when the force moving the stem changes direction. If the valve sticks for instance from D to E in figure 4.1, the controller will try to move the stem longer in the same position, and a stepped curve characteristic will arise.

4.2 Model

4.2.1 Valve model

A valve is simply a narrowing of a pipe, limiting the pipe flow. The size of the narrowing is depending of the valve opening. Assuming that the flow through the valve is frictionless and incompressible and with $z_1 = z_2$, the mass flow $m_v = Av_2$ through a pipe is obtained by a reconstruction of the Bernoulli equation (3.7)

$$m_v = \begin{cases} u_c \bar{C}_v \sqrt{|p_2 - p_1|}, & \text{if} \quad p_2 \geq p_1 \\ -u_c \bar{C}_v \sqrt{|p_2 - p_1|}, & \text{if} \quad p_2 < p_1 \end{cases} \tag{4.1}$$

where $u_c \in (0, 1)$ is the valve opening, $\bar{C}_v = A\sqrt{\frac{2}{\rho}}$ is the valve sizing constant and p_1 and p_2 is the pressure up- and downstream to the valve. The inlet flow v_1 is neglected, a common approximation when modeling valves.

Since all the valves modeled are connected to a separator operating with moles, (4.1) is rewritten to

$$F_v = \begin{cases} u_c C_v \sqrt{|p_2 - p_1|}, & \text{if} \quad p_2 \geq p_1 \\ -u_c C_v \sqrt{|p_2 - p_1|}, & \text{if} \quad p_2 < p_1 \end{cases} \tag{4.2}$$

where $C_v = \frac{1000}{W}\bar{C}_v$ scales the valve constant for mass flow into mole flow.

4.2.2 Sizing constant C_v

When designing a process plant, the sizing of the pipe and valve are important, since they determine the flow from one process component to another. The driving force in pipe flow is the pressure drop at in- and outlet conditions of the pipe. The pressure drop in the pipes are small compared to the pressure drop in the process components and valves. Further, pipe flow dynamics is modeled from heavy flow equations making the total model more complex and time consuming to simulate. Pipe flow dynamics are thus not modeled in this thesis.

To ensure that the valve puts out the wanted controller action, the valve must be sized correctly. A valve that is too small valve will limit pipe flow and saturate the controller. A large valve will result in an unnecessary waste of resources. [Fisher, 2005] describes a *"'step-by-step procedure for the sizing*

of liquid valve,"‘ based on a International Electrotechnical Commission (IEC) standard. Determining the valve constant is a part of this procedure.

The first step is to specify the variables the valve flow coefficient, the process fluid and unit equation constant. There are two types of process fluids, methane and oil. For both fluids the valve flow coefficient is mole flow per second. The second step is to define the piping geometry factor. This step is omitted due to the lack of pipe dynamics in the process model, and this factor is set to 1. The valve sizing constant is finally computed directly from the rewritten valve model (4.2) at maximum valve opening ($u_v = 1$)

$$C_v = \frac{F_v}{\sqrt{\Delta p}} \tag{4.3}$$

where Δp is the less of the maximum and operating pressure drop across the valve and F_v is the worst case mole flow through the vale. This procedure must be repeated for every valve that is modeled.

4.2.3 Stiction model

Stiction is present because of static friction acting on the valve stem. A model of the valve stem dynamics is thus the basis for a stiction model. The valve stem dynamics describes the movement of the valve stem from the moment when the controller sets out a new OP signal until the valve opening (MV-value) is at rest. This position may not be the desired position from the controller due to nonlinearities, in this model stiction and deadband.

[Choudhury et al., 2005] describes the valve stem dynamics by applying Newton's second law, the sum of forces acting on the valve stem is equal to the stem mass times stem acceleration:

$$M_s a_s = M_s \ddot{x_s} = \sum_i F_i = F_a + F_r + F_f + F_p + F_j \tag{4.4}$$

where M_s is mass of the moving parts and x is the relative stem position. $F_a = A_d u_s$ is the force applied by the pneumatic actuator, A_d is the diaphragm area and u_s is the actuator air pressure. $F_r = -kx_s$ is the spring force, k is the spring constant. $F_p = -\alpha \Delta p$ is the force due to fluid pressure drop across the valve, and α is the plug unbalanced area. Because F_p is considerable less than both the friction force, F_f, and the spring force F_r, F_p is omitted, following [Kayihan and Doyle, 2000]. F_j is the extra force required to force the valve into its seat and will also be omitted.

F_f is the friction force and source of stiction, and defined as:

$$F_f = \begin{cases} -F_c sgn(v) - vF_v, & \text{if } v \neq 0 \\ -(F_a + F_r), & \text{if } v = 0 \text{ and } |F_a + F_r| \leq F_s \\ -F_s sgn(F_a + F_r), & \text{if } v = 0 \text{ and } |F_a + F_r| > F_s \end{cases} \tag{4.5}$$

where F_c is the Coulomb friction, F_v is the viscous friction, F_s is the maximum static friction and v is the stem velocity. Different values on the friction constants gives different friction characteristics. A description of friction characteristics is given in figure 4.2, and illustrates that the stiction force must be exceeded before any movement is obtained.

By applying different sizes of the static friction force, different cases of stiction is made.

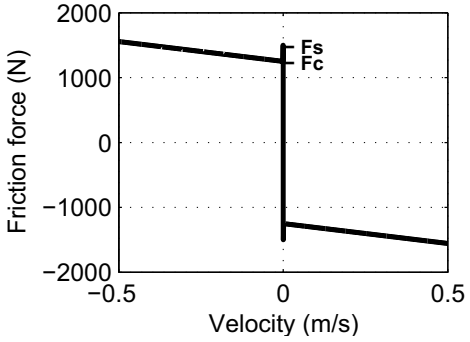

Figure 4.2: Friction force characteristics

Chapter 5

Simulations

The purpose of simulating the production plant model given in chapter 3 with the added valve model with stiction from chapter 4 is to produce data with valve stiction and investigate how valve stiction affects important process variables in the production plant model.

Two cases of are simulated, constant inlet flow with fixed methane fraction (Case1) and constant inlet flow with sinusoidal (Case2) varying methane fraction. The varying input simulate inlet slug flow. For each case, three different sizes of stiction is applied: no, normal and high stiction.

With constant inlet flow and methane fraction the stiction is expected to be easy to verify. If external oscillations enter the process it may be more difficult to detect stiction. Some details about the simulation parameters are now given followed by the results of the simulations.

5.1 Simulation parameters

The production plant model in chapter 3 with the the valve model with stiction from chapter 4 is implemented in `Simulink`™. The model is simulated until an satisfactory period of sample data in steady state conditions is achieved. After 2000 seconds the model had been in steady state conditions for about 1000 seconds. As a result, 2000 seconds is the simulation time for all the cases simulated in this chapter.

The model was quite time consuming to simulate due to the complex process components such as the compressors. As a result, a stiff variable step integration method is applied, *"ode23s"* . The sample rate on the logged data is set to 0.1seconds to fetch all the dynamics of the measured variables.

5.1.1 Physical parameters

A list of all necessary physical parameters is given in table A.1 in the appendix. If not specified with component number, the parameters are equal all

process components. For instance, the liquid oil density ρ_{oilL} yields for both separators, while the separator volumes, V_{sep1} and V_{sep2} are specified for each separator. All the physical parameter values are from the model of [Kylling, 2008].

5.1.2 Controller and valve parameters

The controller parameters with the name of the connected control valve are given in table 5.1. Through initial simulation of the model, the controller parameters used by [Kylling, 2008] achieved satisfactory performance, and his original tuning parameters have been kept to avoid any unnecessary time spent on retuning the whole model.

Table 5.1: Controller parameters with connected control valves

Controller	K_p	T_i	Set point	Control valve
ASCC2	0.22	3	[...]	VRVC2
ASCC3	0.53	12	[...]	VRVC3
LCS11	0.1	200	40.95[m^3]	VLCS1
LCS21	0.1	200	50.04[m^3]	VLCS2
PCS11	$5E^{-10}$	8	30[bar]	VPCS1
PCS12	0.01	0.8	12[bar]	-
PCS21	$3E^{-10}$	8	40[bar]	VPCS2
PCS22	0.01	0.8	15[bar]	-

The valves are sized from the procedure described in section 4.2.2 and the sizing of all the valves is given in table A.2 in the appendices. In the same section, a description of the operating pressure and mass flows in base of the valve size is also given.

5.1.3 Case parameters

[Kylling, 2008] simulates his model with a constant input methane fraction at 0.37 which is a fairly realistic value and used in the case of constant methane fraction throughout this simulation.

The time periods and amplitude of the sine wave are chosen to match the slug flow described in section 1.3. To achieve a variation in inlet pressure, the inlet methane fraction is chosen as the variable to be varied.

The amplitude of the sine wave is 0.1, and its mean value is lowered to 0.25 to avoid saturation of control valves[1]. The time period is 500seconds and corresponds to a frequency of 0.013Hz.

A sinus-wave is an ideal and linear disturbance and should gain information on how a large disturbance propagate through the process components. Since

[1] A saturated control valve can introduce oscillations, which can give detection of false stiction.

the sinus-wave is linear, it should not destroy the nonlinear shapes in measured data produced by stiction.

Table 5.2 summarizes the parameters for the two cases.

Table 5.2: Parameters of simulated cases

Case #	Descr.	Mean	Amplitude	Time period
Case1	Constant	0.37	0	∞
Case2	Sinus	0.25	0.1	$500sec$

5.1.4 Stiction sizes

Three different sizes of stiction is applied to each case of the inlet methane fraction to study the effects of increasing stiction on controlled variables. The size of the stiction is varied by changing the stiction force in the friction model in equation (4.5). The stiction sizes in Newton and corresponding percentage controller change in stick- and jumpband are given in table 5.3.

Table 5.3: Sizes of the stiction cases

	No stiction	Normal stiction	High stiction
F_s	$1250N$	$1750N$	$2250N$
Stickband	5%	5%	5%
Jumpband	0%	1%	2%

When no stiction is applied, the only nonlinearity is deadband, the valve stem does not jump when it starts to move after it has been stuck. No oscillations are thus expected to occur in non-integrating processes due to deadband only.

5.2 Constant input methane fraction

The purpose of simulating the production plant model with a constant input methane fraction is to investigate how stiction affects other process components and to produce process data with stiction for testing of an algorithm that detects stiction.

Classical MV-OP and PV-OP plots are presented to verify the presence of stiction.

5.2.1 Key variables

Figure 5.1 shows the behavior of the key variables in the simulated production plant model for the three cases of stiction with constant input methane fraction. From the figure it is clear that oscillations occur when stiction is present. When no stiction is present, the variables are nearly constant.

As described in chapter 2, special shapes for process variables arise in the presence of stiction. These shapes should be recognized in the pressure and volume control error signals. In figure 5.1(b), the shapes of the pressure control error are best recognized for normal stiction. The pressure control error form an exponential rice and decay shaped oscillation, which is characteristic for PV data from non-integrating processes with stiction. The pressure model acts like a filter that smooths the pulse in the MV signal. See figure B.1 in the appendices for time plot of the MV and OP data. When high stiction is present the exponential rice and decay are harder to verify visually.

The shape of stiction induced oscillations in PV data from an integrating process normally is triangular due to integration of a square pulse in the MV data. In figure 5.1(a), the triangular shapes of the volume control error are best recognized in the high stiction case. With normal stiction there are small oscillations in the increasing part of the volume control error signal. The lack of the pure triangular shapes can be explained from the tuning of the volume controller which is not tuned tightly because of reasons described in section 3.5.3.

Note that the rice time is slower than the decay time in the normal stiction case for both the pressure and volume controller. An explanation of this is that when the pressure or volume in the separator is to low, the only way of increasing it is to wait for more crude oil to enter since negative flow is not allowed in the process. When the pressure or volume is to high, the controller effectively decreases the pressure or volume by letting more gas or oil out of the separator.

From Separator 1, the oscillations spread to other components in the process such as the connected compressor and the gas turbine controlling the shaft speed for the controllers. Figure 5.1(c) and 5.1(d) shows the outlet pressure of Compressor 2 and the shaft speed of the shaft that drives the tho compressors in the production plant model.

Table 5.4 presents the amplitudes and the time periods of the largest oscillations for all the variables in figure 5.1. From the table it is confirmed that the oscillations in the pressure controller spread to the compressor. The time periods of the oscillations that occurs in the pressure controller are very similar to the time periods of the oscillations in the compressor and shaft speed.

The amplitudes increase with increasing stiction for all variables except the volume control error where the amplitude is equal for normal and high stiction.

A 100% increase stiction (from normal to high) size results in a 200% increase in the amplitude for the oscillation in the compressor shaft speed . For the compressor outlet pressure the increase is 141% and for the comtrol error pressure 69%. These results indicate that an increase in stiction has largest effect on the compressor shaft speed. However, it should be noted that the amplitude of the shaft speed oscillation is only 0.39RPM which is

relatively small.

A comparison of the control pressure error and the compressor outlet pressure indicate that the oscillation amplitudes from stiction are damped in the compressor (damping of 54% in the normal stiction case and 34% in the high stiction case). This may be because of the pressure rise in the compressor.

Table 5.4: Amplitudes and time periods (A/T) for stiction induced oscillations, constant methane fraction

Fig#	No stiction	Normal stiction	High stiction	Units
5.1(a)	$\infty/0$	339/0.30	77/0.30	[sec/m^3]
5.1(b)	$\infty/0$	101/0.26	37/0.44	[sec/bar]
5.1(c)	$\infty/0$	100/0.12	39/0.29	[sec/bar]
5.1(d)	$\infty/0$	100/0.13	40/0.39	[sec/RPM]

5.2.2 MV-OP and PV-OP plots

The classical MV-OP and PV-OP plots for both volume and pressure control are presented in figure 5.2 and 5.3. The case with no stiction is omitted here since no oscillations and no controller variation are present for this case, producing only a single dot in these plots.

In figure 5.2 stiction is recognized by the rectangular shapes. The sizes of the stick- and jumpband coincide with the sizes in table 5.3. As described in section 4.1, the length of horizontal lines gives the size of the stickband. The length of the vertical lines give the size of the jumpband.

By increasing the stiction, the increase in the jumpband is more visible since the relative increase is larger for the jumpband compared to the stickband. The stickband is the sum of both deadband and stiction.

Figure 5.2 also shows that there is no difference in the the shape and size of the MV-OP plots for the volume and pressure controller. This is because the same valve model is applied to the two different control loops. MV-OP plots are thus a valuable tool to confirm and quantify stiction.

For the PV-OP plots in figure 5.3, the shapes differ depending on the control loop. An ellipse is observed for the pressure control loop in figure 5.3(a) and 5.3(b) and indicates that stiction is present. The ellipse is deformed in the upper left part of the ellipse in figure 5.3(a). This is because the different shapes in the pressure rice and decrease observed in section 5.2.1.

In the PV-OP plot from the volume control loop there is harder to recognize the ellipse, see figure 5.2(c) and 5.3(d). The ellipses are more narrow and have sharper edges. From correspondence with [Hovd, 2009] this can be explained from the fact that an integrating process shifts the phase 90°. To shift the phase by 90° is equal to view an ellipse observed from process data with 0° phase shift from the side. In an ideal case, a single line will be visible in the PV-OP plot of an integrating process. There is not a single line in

figure 5.2(c) and 5.3(d) because the volume process is not a purely integrating process. An idea on how to omit this problem is presented in chapter 7.

As described in section 2.3, the width of the ellipse in the OP direction at the mean of the ellipse can quantify stiction. Figure 5.3(b) is the only case where the with of the ellipse is near to the correct value at 2%. The deformed upper shape of the ellipse in figure 5.3(a) increases the width of the ellipse, while the phase shift for the volume process decreases the width of the ellipses, see figure 5.2(c) and 5.3(d).

From the uncertainties described, to quantify and detect stiction from a PV-OP plot only should be done with caution.

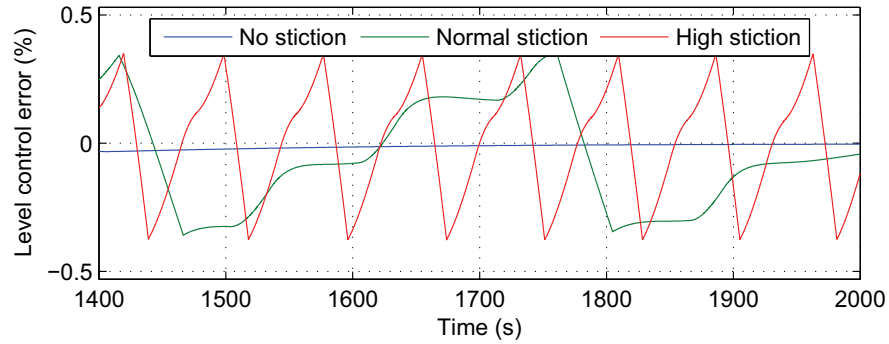

(a) Separator 1 volume control error.

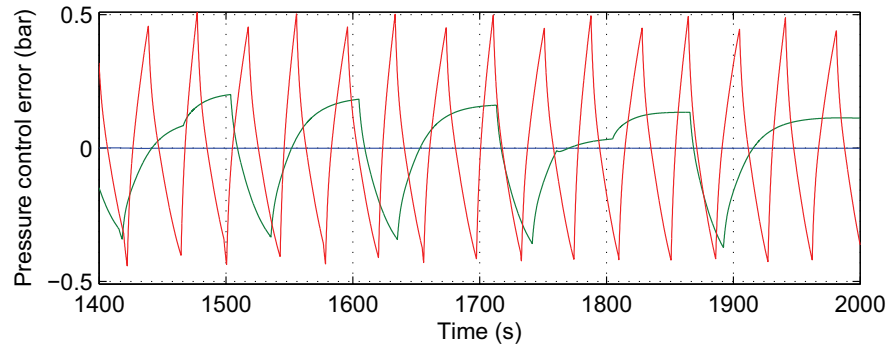

(b) Separator 1 pressure control error.

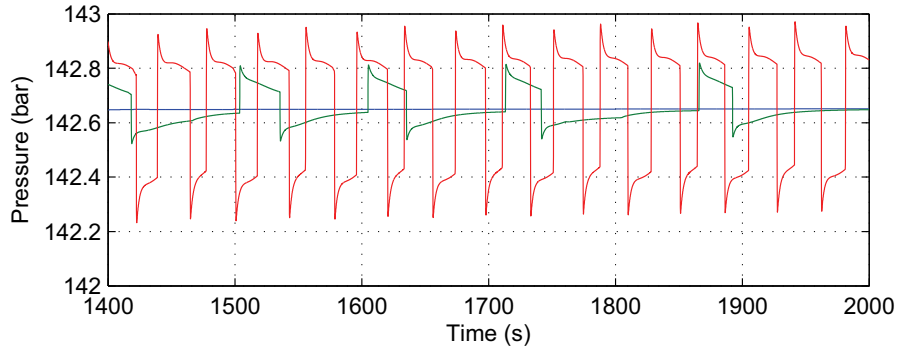

(c) Compressor 2 output pressure.

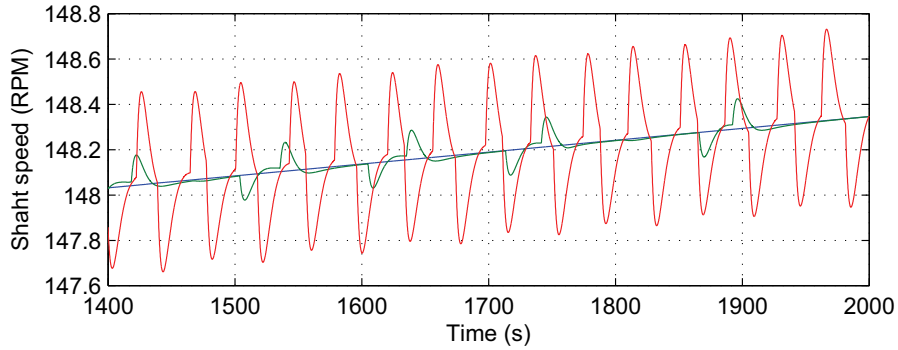

(d) Gas turbine shaft speed.

Figure 5.1: Key process variables, constant methane fraction

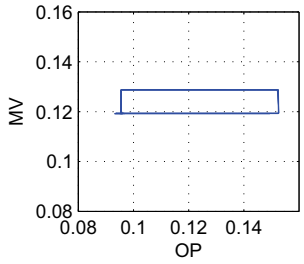

(a) Pressure control, normal stiction.

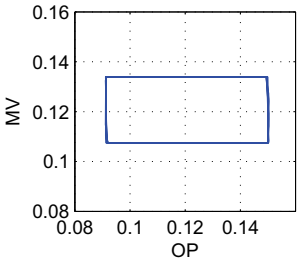

(b) Pressure control, high stiction.

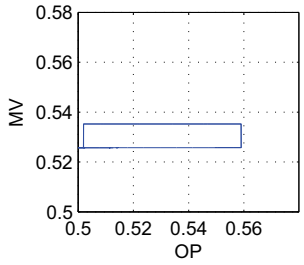

(c) Volume control, normal stiction.

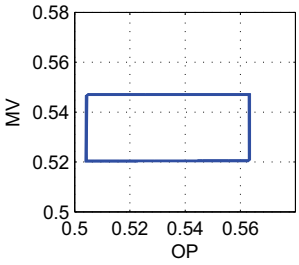

(d) Volume control, high stiction.

Figure 5.2: MV-OP plots, constant methane fraction

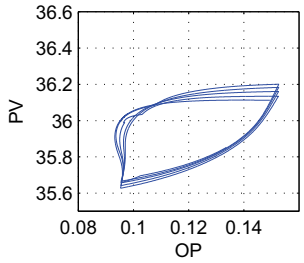

(a) Pressure control, normal stiction.

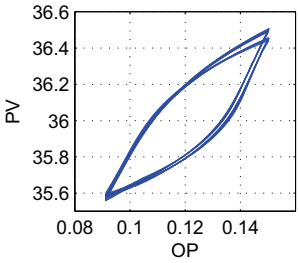

(b) Pressure control, high stiction.

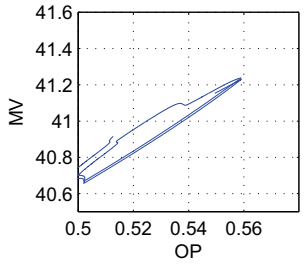

(c) Volume control, normal stiction.

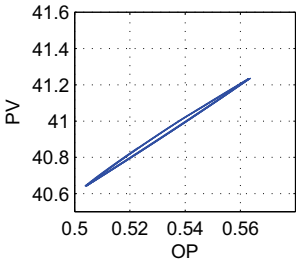

(d) Volume control, high stiction.

Figure 5.3: PV-OP plots, constant methane fraction

5.3 Sinusoidal methane fraction

To simulate the production production plant model with a sinusoidal input methane fraction will provide information about how the stiction oscillations are affected by an linear disturbance. Data from the simulation will also be used in a test of an algorithm for stiction detection.

Further, it will be interesting to see how the MV-OP and PV-OP plots vary compared to the case with a constant input. The disturbance will introduce more variation of controller output and these plots are expected to have larger shapes. It should be possible to distinguish the shapes from the linear disturbance from the nonlinear shapes characteristic for stiction.

5.3.1 Key variables

Figure 5.4 shows the behavior of the key variables in the simulated production plant model for the three cases of stiction with sinusoidal input methane fraction. As seen, all the key variables are largely affected of the sinusoidal input methane fraction. The variable that is least affected of the input is the shaft speed of the gas turbine, see figure 5.4(d).

Small oscillations with amplitudes and time periods similar to the stiction induced oscillations observed in section 5.2 occur in the case of high stiction. Only one period of the input sine wave is plotted to give a better view of these small oscillations.

With no and normal stiction, there is no small oscillations in the volume control error in figure 5.4(a). High stiction introduces some scattered small oscillations. The time period, amplitude and form of these oscillations vary during the simulation, making them hard to quantify. The reason for this is most likely the the weakly tuned volume controllers.

In figure 5.4(b) small oscillations is present between 1500 and 1800 seconds for the case of high stiction. Some of the shapes in these oscillations are the exponential rice and decay shapes that is characteristic for stiction. As in section 5.2, the controller can only affect the pressure if it is too high. When the pressure is below the set point, the only way of increasing the pressure is to wait for more crude oil to enter the separator, and the controller output is zero during this period, see figure B.2(c) in the appendices. This explains why the pressure control error follows the inlet disturbance before and after the period of small oscillations and why a saturated controller can introduce oscillations in the controlled variable.

The small oscillations in the separator pressure spread to the compressor pressure and shaft speed in figure 5.4(c) and 5.4(d). The size and form of the oscillations are similar to the ones observed in section 5.2 for high stiction.

The large increase in the compressor pressure is present due to the inlet disturbance that propagates through the pressure controller. However, the increase in pressure does not affect the shaft speed to the same extent. This

may be because the disturbance is so slow that the compressor is within its working point during the whole simulation. The small oscillations do however propagate to the shaft speed, indicating a high-pass filtering effect from the compressor pressure to the compressor torque.

5.3.2 MV-OP and PV-OP

Stiction can easily be verified from the MV-OP plot in figure 5.5. In figure 5.5(a) and 5.5(d), the MV-OP shapes almost match the ideal shape in figure 4.1. The jump in the MV value in the lower right and upper left corners of both the figures confirms the presence of stiction. In the increasing part of both the figures there is a continuous valve stem movement, while for the decreasing part of figure 5.5(a) the MV value stick and slips in the same direction, producing a stepped curve.

These stepped curves are more dominating in the cases for high stiction, see figure 5.5(b) and 5.5(d). An important difference from the case with constant input in section 5.2.2 is that the deadband does not occur when the valve sticks and slips in the same direction. In industry, this stepped curve is uncommon according to [Choudhury et al., 2005].

A ellipsoidal form is viewed in all the plots of figure 5.6 except in figure 5.6(a) where process dynamics and the input disturbance destroys the ellipse.

In figure 5.6(b), two parallel shifted ellipses are observed. The sizes of these ellipses are equal to the ones observed in section 5.2.2. The ellipses are affected by noise and can be hard to detect by an automatic method as the one purposed by [Choudhury et al., 2006].

In difference from section 5.2.2, the PV-OP plots in figure 5.6(c) and 5.6(d) now take the form of an ellipse. The ellipse in figure 5.6(c) are not sharp-edged, indicating that there is only linear oscillations behind the ellipse shape. In figure 5.6(d) the shapes of the ellipse are sharp. It is however likely that these ellipses arises from the linear disturbance since the width of the ellipses does not increase with the increasing stiction. The with of the ellipse is also ten times larger then the stiction for the normal stiction case and five times larger in the high stiction case.

There is also in the case of sinusoidal input disturbance hard to detect and quantify stiction from PV-OP plots only.

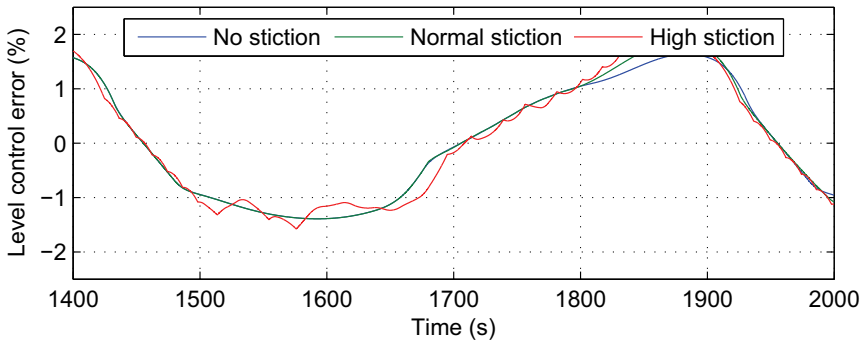

(a) Volume control error.

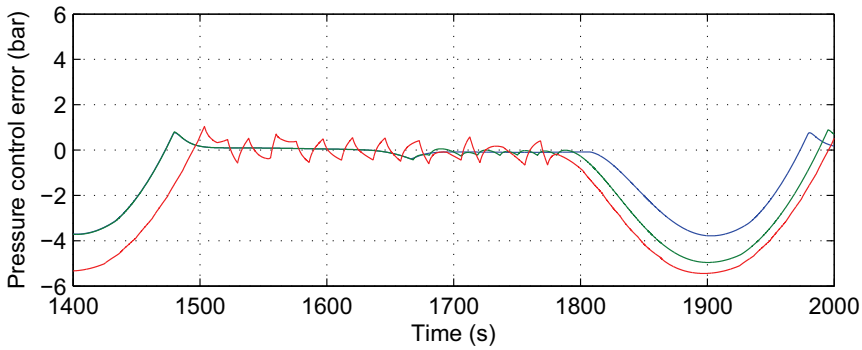

(b) Pressure control error.

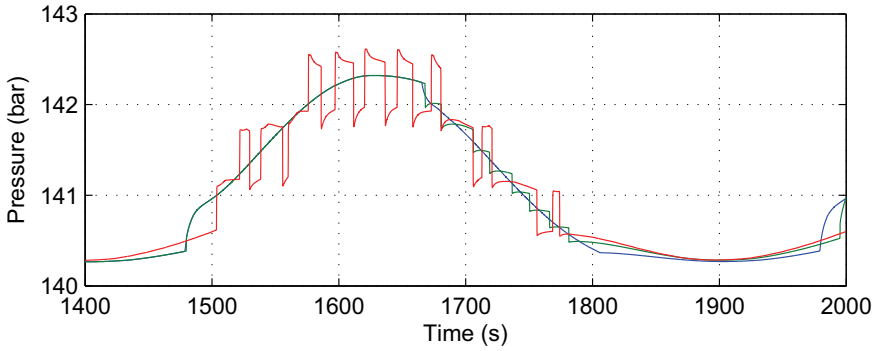

(c) Compressor 2 output pressure.

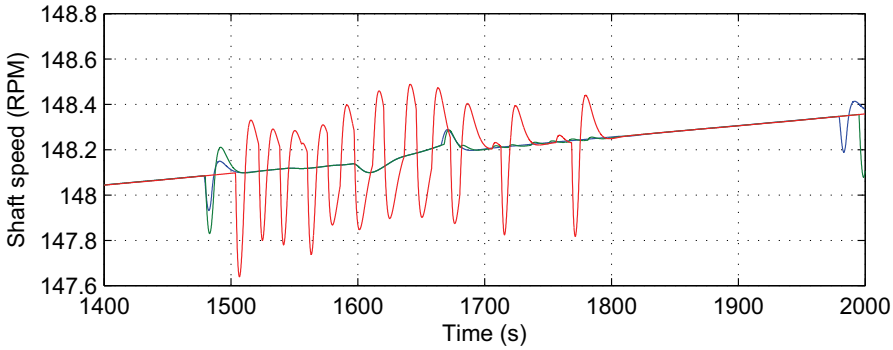

(d) Gas turbine shaft speed.

Figure 5.4: Key process variables, sinusoidal methane fraction

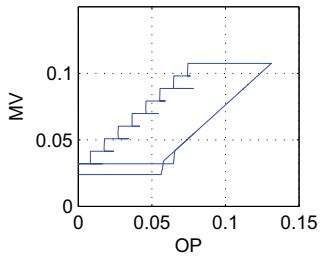

(a) Pressure control, normal stiction.

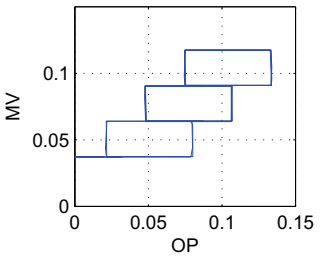

(b) Pressure control, high stiction.

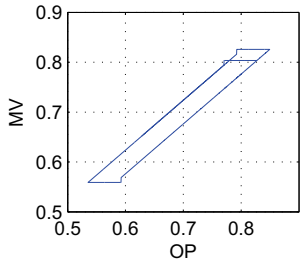

(c) Volume control, normal stiction.

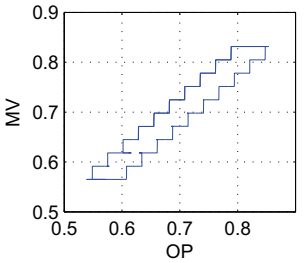

(d) Volume control, high stiction.

Figure 5.5: MV-OP plots, sinusoidal methane fraction

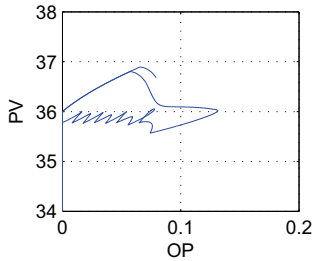

(a) Pressure control, normal stiction.

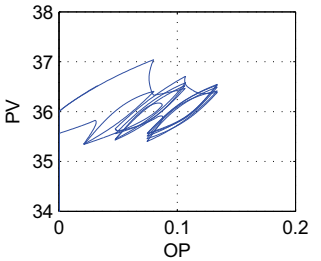

(b) Pressure control, high stiction.

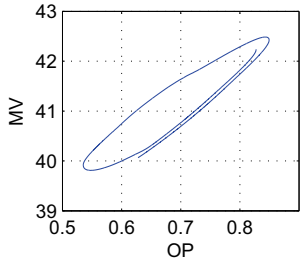

(c) Volume control, normal stiction.

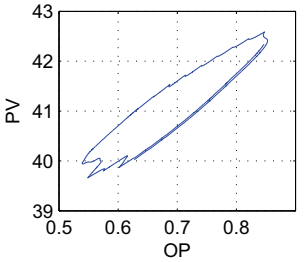

(d) Volume control, high stiction.

Figure 5.6: PV-OP plots, sinusoidal methane fraction

Chapter 6

Algorithm for stiction detection

This chapter presents an algorithm that automatically detects stiction from routine operating data. The algorithm is not complete, but is a nice stepping stone for further development as part of a new feature in the logging system for Siemens.

The chapter initially lists some criteria for the algorithm given by the author in collaboration with Siemens, followed by a presentation of the algorithm. The algorithm is further tested on some ideal data sets: the data produced in chapter 5 and some real data from an oil and gas production plant. The chapter ends with some suggestions for improvements of the algorithm.

6.1 Criteria for algorithm

In collaboration with Siemens, the following criteria are defined for the algorithm developed in this chapter:

- **Applicable to all process types.** The algorithm should be applicable to all the process types at a general process plant to avoid extra work specifying process type and tuning of the algorithm for each control valve and process.

- **Low computational burden.** Since there can be several thousand control valves at a process plant, a small increase in computational power at each valve will require a huge total investment.

- **Handle a varying sample time.** The logging system of Siemens only logs a measurement when there is a significant change in the measured value. The algorithm is thought to be a feature in the logging system and should thus use data directly form the logging system.

In addition to these criteria, the algorithm should be automatic and installable online to provide the operator with real-time information.

6.2 Choice of principle

To meet the first criteria, the test results of [Horch, 2007] are studied. He tested many of the methods described in chapter 2 on a variety of datasets from different processes with and without stiction. He compares how correct the different methods conclude on stiction appearance on all the datasets. He noted that there is not one method that covers all the applied data sets. The top five methods from this comparison is method number *iii, vii, xi, x* and *xi* following the method numbering from table 2.1.

From the top five methods only method number *iii*, *vii* and *xi* are based on time domain analysis. To transform the data into the frequency domain would require an increase in computational load. Methods that use time domain data only, should thus be chosen in order to meet the criteria of low computational burden.

[Kvam, 2008] states that the compression of data done by the logging system of Siemens makes any system identification from the compressed data hard. As a result, stiction detection methods based on identification are not relevant for usage. Together with the fact that an identification also require some computational power, the only methods left are method number *iii* (the method of [Singhal and Salsbury, 2005]) and *vii* (the method of [Rossi and Scali, 2004]).

The method of [Singhal and Salsbury, 2005] exploits the difference in the left and right half cycle integral when stiction is present. The integral of a function $f(t)$ between two discrete data points t_1 and t_2 can easily be computed using numerical trapezoidal integration defined in [Egeland and Gravdahl, 2003]

$$\int_{t_1}^{t_2} f(t) \approx \frac{1}{2}\big(f(t_1) + f(t_2)\big)(t_2 - t_1) \tag{6.1}$$

By computing this integral for each measurement present and keeping track of the maximum or minimum of the half cycle, the method of [Singhal and Salsbury, 2005] can handle a varying sample time $(t_2 - t_1)$. This nice property fulfills the last criteria in section 6.1.

In addition, the method of [Singhal and Salsbury, 2005] concludes more correct than the method of [Rossi and Scali, 2004] in the tesing done by [Horch, 2007]. The method of [Singhal and Salsbury, 2005] is the choice of principle for the algorithm developed in this chapter.

It should be noted that the method of [Singhal and Salsbury, 2005] is patented, according to [Horch, 2007]. This can complicate use in a future

Siemens implementation. However, the author chooses to ignore this fact since the method is published and no details about any commercial implementation of the method is given in the published paper. As a result, before a future commercial use of the proposed algorithm, the details of the patent attached to the method of [Singhal and Salsbury, 2005] should be further studied.

6.3 Algorithm

The algorithm input is a controller error data set, Y, the output is a stiction index (R) where values greater than one indicates that stiction is present in the controller error data set. The algorithm is written in `Matlab`™. It makes use of the general *for*- loop and the `Matlab`™ function *sign()*.[1]. The algorithm is presented in a general pseudo code, see algorithm 1, and should thus be implementable in most industrial programming languages.

The algorithm initially gets the length of the data set before the *for* loop computes the integrals necessary for the stiction index. The loop iterates over all values in the data set except the first and last value.

For an online implementation, the for loop can be exchanged with an infinite while loop that iterates one time for each new measurement present. The loop index i must then be replaced by a counter.

Inside the loop, the slope sign is computed from the sign of the difference between present and previous data sample, see line 4. The slope sign indicates whether the controller error increases (SIGN= 1) or decreases (SIGN= -1). Before any integral value is detected, a zero crossing must occur. If a zero crossing is present and no integral is computed, a new iteration is done without any action, see line 8.

Further, if the controller error is increasing, the integral value between the present and next data sample is added to the integral value A_1 using the trapezoidal integration in equation (6.1), see line 17. When a local maximum is reached, the slope changes sign and the integration values are added to A_2, see line 19.

When a zero crossing is detected and both A_1 and A_2 are non zero, R is computed. Since R is defined as the ratio of integrals before and after a peak between two zero crossings, a test is needed to distinguish between positive and negative integral values. Line $9 - 12$ ensures this. If the integral values are negative, A_2 is the first integral. If the integral values are positive, A_1 is the first integral. Finally, the integral values are reset, and a new integral computation can begin, see line $14 - 15$.

During testing, all the computed values of R and integrals are stored to ease the analysis of the algorithm. The mean and standard deviation of approximately 20 values of R are computed to assess the uncertainty of the index.

[1] *sign()* returns 1 for positive sign, -1 for negative sign and 0 for zero value

Algorithm 1 Field stiction detector, initial

N ← SIZE OF Y
$A_1 \leftarrow 0$
$A_2 \leftarrow 0$
for $i = 2$ to N−1 **do**
  SIGN ← $sign(Y(i) - Y(i-1))$
  if ZERO CROSS BETWEEN $Y(i)$ and $Y(i+1)$ **then**
    if (A_1 OR A_2) = ZERO **then**
      BREAK
    else if $A_1 > 0$ **then**
      $R \leftarrow \frac{A_1}{A_2}$
    else if $A_1 < 0$ **then**
      $R \leftarrow \frac{A_2}{A_1}$
    end if
    $A_1 \leftarrow 0$
    $A_2 \leftarrow 0$
  else if SIGN = 1 **then**
    $A_1 \leftarrow A_1 + 0.5(Y(i) + Y(i+1))(t_{i+1} - t_i)$
  else if SIGN = −1 **then**
    $A_2 \leftarrow A_2 + 0.5(Y(i) + Y(i+1))(t_{i+1} - t_i)$
  end if
end for

6.4 Applied on ideal data

Before the algorithm is applied to data from the simulation in chapter 5 and real data from industry, the algorithm is tested on two sets of idealized data: an ideal stiction shape and a sinus wave.

The ideal stiction shapes are the exponential rice and decay in the PV data, a shape that characterizes stiction. These shapes are produced from simulation of a simple PI controlled first order process with high stiction in the control valve. The controller structure is equal to the general control structure in figure 1.2. The process $C(s)$ and controller $G(s)$ is defined as

$$G(s) = \frac{3}{10s+1}, \quad C(s) = 0.4\Big(\frac{10s+1}{10s}\Big) \tag{6.2}$$

This simple process is simulated in `Simulink`™ for 600s using the *ode23s* integration method and a 0.1 seconds sample time. An initial step in reference is applied to invoke controller usage.

The sine wave has a time period of 50 seconds and an amplitude of 0.075. The results of the algorithm tests on the the ideal data sets are presented in figure 6.1. The mean of the stiction index and its standard deviation are given in the figure text. The integral areas computed by the algorithm are colored

to red (A_1) and blue (A_2) following the notation of the pseudocode.

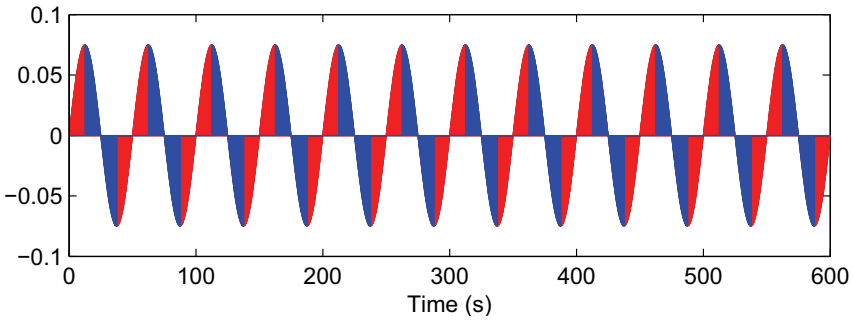

(a) Sine wave, $\bar{R} = 1.03 \pm 0.00$

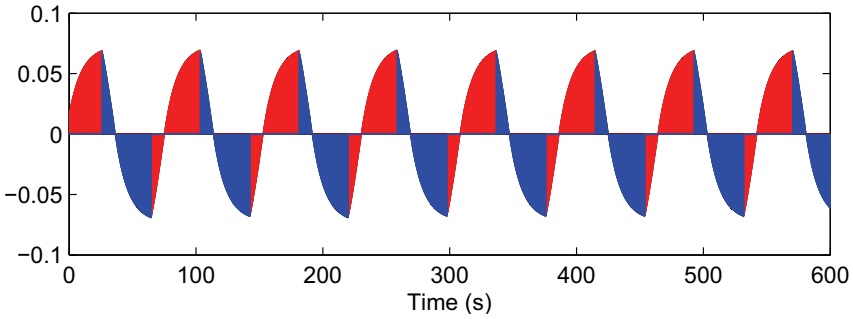

(b) PI controlled first order process with high stiction, $\bar{R} = 3.71 \pm 0.06$

Figure 6.1: Algorithm test on ideal data, high stiction.

As expected, the two areas in figure 6.1(a) are equal and the mean value of R is nearly one for the sinus wave. The small deviation from one is present because of numerical integral errors from the trapezoidal rule.

From figure 6.1(b) it is clear that the two areas before and after the peaks in the stiction shapes are not equal which result a mean value of R larger than one. As a result, the algorithm concludes correct for the two ideal data sets presented in this section.

An important remark is that the size of the stiction index cannot quantify the size of the stiction. A decrease in stiction or a decrease in controller gain both result in an increase in the stiction index, see figure B.3 in the appendices.

6.5 Applied on data from production plant model

The algorithm proposed in this chapter is now applied on the pressure and level control errors from the simulation of the production process model in chapter 5. The algorithm is tested on data from both constant and sinusoidal methane fraction for all stiction cases.

The tests are done to gain information about the behavior of the algorithm when applied to interacting and non-integrating processes with both constant and varying inputs.

6.5.1 Constant methane fraction

The mean and standard deviation of the stiction index from the tests on data with a constant input methane fraction are presented in table 6.1. The case with no stiction for the constant methane fraction is omitted since the simulation produced no oscillations for this case.

For the level process the algorithm cannot conclude safely that stiction is present. In the normal stiction case, the value is nearly one and the stiction index concludes with an aggressive controller which is incorrect. The conclusion for the level process with high stiction is vague since the mean value has a large standard deviation.

From the results of the pressure process the algorithm can conclude with presence of stiction since R is much larger then one in both the normal and high stiction case. The large standard deviation in the normal stiction case arises because of the different shapes in the control error signal above and below zero, see figure 5.1(a).

Table 6.1: Mean and standard deviation of stiction index ($\bar{R} \pm \sigma_{\bar{R}}$), production process model with constant input

Process type	**Normal stiction**	**High stiction**
Level	0.94 ± 0.71	1.74 ± 1.36
Pressure	14.63 ± 17.13	4.09 ± 1.80

6.5.2 Sinusoidal input methane fraction

Table 6.2 give the test results of the algorithm applied on data from simulation of the production process model with a sinusoidal input methane fraction.

The results from the level process are again hard to conclude from. For the case of no stiction, the mean value of R is even higher than the value of R in the high stiction case for the constant input. The input sine wave is deshaped from process controller action and process dynamics.

Due to the large influence in the pressure from the varying methane input fraction, the values of R are below one in the case of no and normal stiction for the pressure process. For high stiction the algorithm concludes correct, but the high standard deviation indicate that there is large uncertainty in this conclusion.

Table 6.2: Mean and standard deviation of stiction index ($\bar{R} \pm \sigma_{\bar{R}}$), production process model with sinusoidal input

Process type	No stiction	Normal stiction	High stiction
Level	1.80 ± 0.63	1.63 ± 0.40	0.89 ± 0.12
Pressure	0.46 ± 0.59	0.87 ± 0.89	3.06 ± 2.25

6.6 Applied on real process data

The real case data available for testing of the purposed algorithm are from a level and pressure control valve at a production plant for oil and gas. The level control valve is reported to have stiction in [Torpe and Dessen] while the pressure control valve is part of a pressure controller close to the level control valve with stiction.

Ideally, data from a pressure control valve with reported stiction should be available, since the algorithm is reported to conclude incorrect on data from from level processes. But it has proven to be hard to get such data from Siemens. Anyway, the tests on real case data will give valuable results in how the algorithm copes with a varying sample time and noise.

As stated in in section 6.1, the logging strategy of the Siemens logging system results in a varying sample time in the logged data. The mean sample time and standard deviation is 6.84 ± 3.18 seconds for the level data and 91.59 ± 37.04 seconds for the pressure data.

Table 6.3 lists the mean and standard deviation of the stiction index from the controller error data sets described above. In addition, the mean and standard deviation of the oscillation time period and amplitude are given to gain some more info about the datasets. Figure 6.2 shows the datasets with the computed integral value in the same way as in figure 6.1. A line is drawn for each integral computed and the colors distinguish the two integral areas A_1 and A_2.

Table 6.3: Mean and standard deviation of stiction index ($\bar{R}$), time periods ($\bar{T}_{osc}$) and amplitude ($\bar{A}_{osc}$) of oscillations from real data

Process type	$\bar{R}$	$\bar{T}_{osc}$	$\bar{A}_{osc}$
Level	1.80 ± 1.32	188.52 ± 151.80	2.25 ± 1.38
Pressure	3.14 ± 2.74	670.30 ± 919.48	0.02 ± 0.01

From the values of the stiction index in table 6.3 there is difficult to conclude about the presence of sticion, especially for the data from the level process. However, the oscillation time period for the level data are in the area of the time periods of the stiction induced oscillations in chapter 5. The sizes of the amplitudes are in the range of the amplitudes from the sine disturbances indicating that the oscillations arise from a disturbance.

The mean of the stiction index for the pressure data is 3.14 and indicates that stiction is present, but the long time periods and small amplitudes complicates the conclusion. Because of the small amplitudes, there is likely that the real pressure is constant, but affected by measurement noise.

To assess the performance of the algorithm regarding noise and a varying sample time, figure 6.2 is studied. For both the processes, the algorithm copes with the varying sample time, but it seems like the sample time is in general too long in the pressure data. If the oscillations consist of only one sample, the increasing and decreasing integral area cannot be computed. Interpolation can solve this by introducing more samples during the oscillation time period.

Noise is present in both figure 6.2(a) and 6.2(b) and result in a change of the derivative sign before a peak is reached. Because of this, the decreasing integral areas can be added during a increasing time trend and vice versa which leads to an incorrect value of the stiction index. A discrete pre-filtering of the data samples can solve this, but can be hard to apply on data with a varying sample time.

6.7 Improvements

Based on the results and discussion of the tests in section 6.4 some improvements of the algorithm are suggested:

- Additional functionality must be made to handle integrating processes.
- The problem of noise must be investigated and solved, discrete pre-filtering can be a solution.
- The algorithm should give more correct conclusions in the presence of large disturbances. Detection and comparing of the different time periods present in the data set can give valuable additional information.

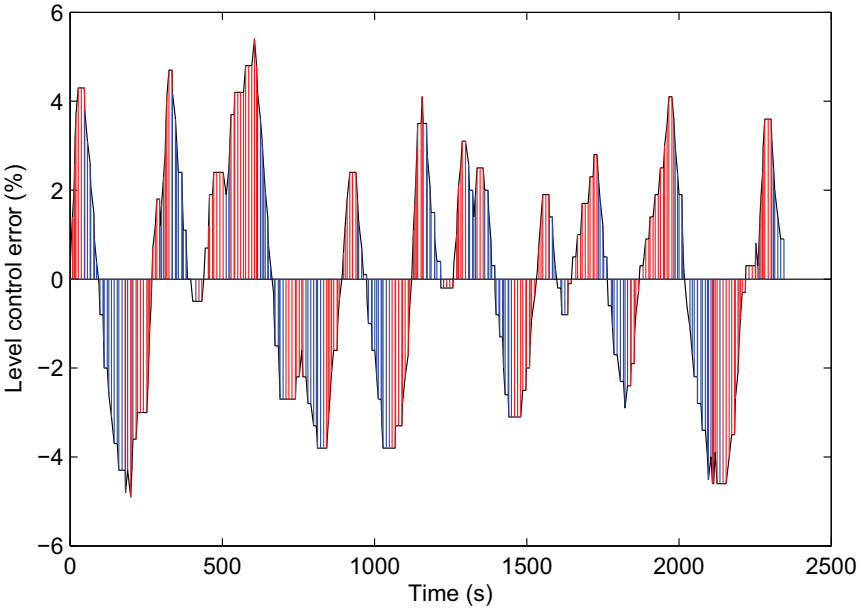

(a) Level process, $\bar{R} = 1.80 \pm 1.32$

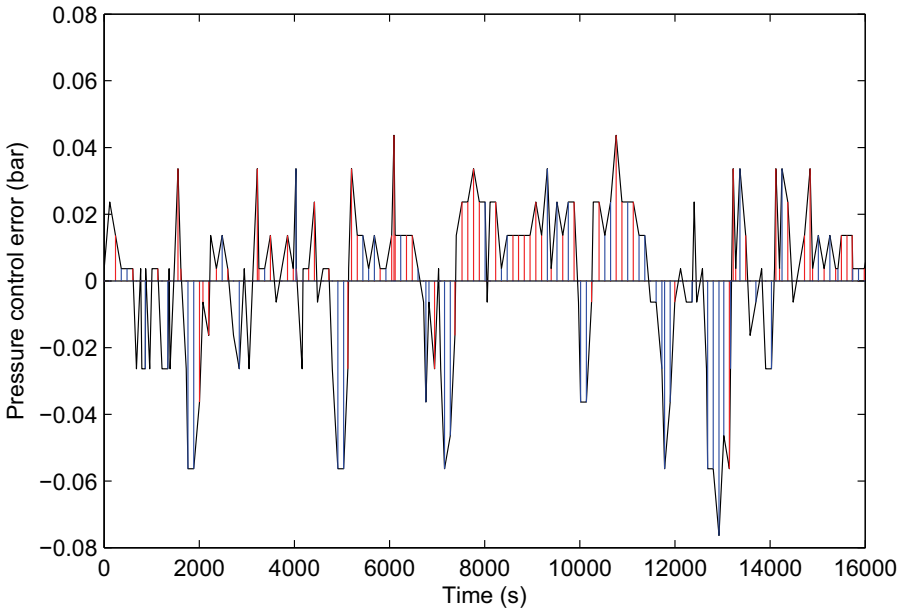

(b) Pressure process, $\bar{R} = 3.14 \pm 2.74$

Figure 6.2: Algorithm test on real data

Chapter 7

New principles for stiction detection

The results from the previous chapters show that there is hard to detect stiction in a PV-OP plot for integrating processes. This chapter presents some ideas on how to solve this.

7.1 Background

Use of PV-OP plots are one of the classical ways in industrial practice to detect stiction in a control loop from routine operating data, according to [Choudhury et al., 2006].

When stiction induced oscillations are present, the PV-OP plot takes the shape of an ellipse. The assumption for these shapes to occur is that the process time constant is significantly shorter than the time periods of the stiction induced oscillations. For non-integrating processes the phase-lag then is 0° between the OP and PV data. Any oscillation with a significant longer time periods than the process dynamics will then make shapes in the PV-OP plot.

There has been little research on how these shapes develop in data from integrating processes. Integrating processes introduce 90° phase lag between the OP and PV data. [Hovd, 2009] states that this phase lag results in a 90° twist of the circle or ellipse shapes in the PV-OP plot. The twist leads to a more narrow ellipse or even a single line in an ideal case.

Two ideas on how to regain the ellipse in a PV-OP plot from an integrating process are now presented.

7.2 Description of ideas

7.2.1 Idea number 1

[Hovd, 2009] suggests to plot OP data against time shifted PV data to regain the shapes of the ellipse. The time shift of N samples of a general vector y is simply

$$y_{ts}(t) = y(t + N) \tag{7.1}$$

7.2.2 Idea number 2

Another idea is to plot OP data against filtered PV data. If the filter can change the 90° phase lag between PV and OP data back to 0° phase lag, the ellipse should be regained in the PV-OP plot.

The filter basis is a continuous first order high-pass filter

$$H(s) = \frac{s}{s + \tau} \tag{7.2}$$

where τ is the filter time constant. If the time constant is large, the filter can be viewed as a derivator at low frequencies which adds a 90° positive phase lag to the filtered data . A discrete version of the high-pass filter is

$$y(t) = \alpha y(t - 1) + \alpha(x(t) - x(t - 1)), \quad \alpha = \frac{\tau}{\tau + T_s} \tag{7.3}$$

where $x(t)$ is the filter input, $y(t)$ is the filter output and T_s is the sample time of the discrete data. Some trial and error are done to find a filter constant τ that regains the ellipse shape.

7.3 Results

Both the ideas from the previous section are tested on data from an ideal integrating process. The valve stiction model applied is the model from chapter 4. The high stiction case from chapter 5 is used to enlarge the stiction effects.

The ideal integrating process and controller is

$$G_I(s) = \frac{3}{10s}, \quad C(s) = 0.2\Big(\frac{400s + 1}{400s}\Big) \tag{7.4}$$

Negative controller usage and PV values are allowed to force the ideal integrating process to produce oscillations. The ideal process is simulated in 2000 seconds. The time plot of the MV and OP data is given in B.4 in the appendices confirms the characteristic time domain shapes for an integrating process with stiction.

7.3.1 Idea number 1

Some simple trial and error testing is done to find a N that regained the ellipse. Figure 7.1 shows the PV-OP plots for different values of N.

Small values of N only increase the ellipse shape, see figure 7.1(b). For larger N, the shapes take more a form of a rectangle, and the ellipse shapes are smoothened out which make the ellipse shapes harder to detect. The width of the rectangles increase when N is increased.

The search for correct values of N to regain the ellipse must most likely be repeated if the oscillation time period changes. Proper guidelines to find such an N for different time periods should be developed before the performance of this idea could be concluded.

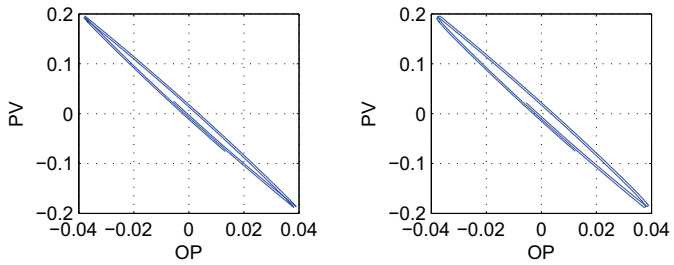

(a) N = 10.

(b) N = 50.

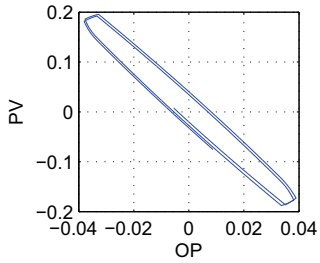

(c) N = 200.

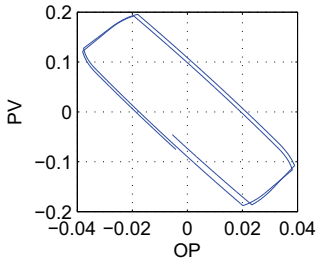

(d) N = 400.

Figure 7.1: PV-OP plot with time delayed PV data, ideal integrating process

7.3.2 Idea number 2

Figure 7.2 shows the OP data plotted against non-filtered PV-data from the ideal integrating process. Filter time constants of 100 and 50 give different sizes of the hidden ellipse without changing the shape of the ellipse, see figure 7.2(b) and 7.2(c). When the filter time constant is decreased to 10, the shape of the ellipse is changed, which indicates that the phase lag is above 90°.

Data from the level process part of the production plant model simulated in chapter 5 are also applied to this idea, see figure 7.3. The filter parameters are equal to the ideal case to make comparison the results from the different

cases possible. For the filter time constants of 100 and 50 in figure 7.3(b) and 7.3(c), the ellipses develop in a similar case as in figure 7.2, the width increases without changing the shape of the ellipse.

In figure 7.3(d), the upper ellipse shape is changed. This may be due to the little break in the controller volume error in figure 5.1(a). The little break is amplified because of the small filter constant. If more small changes such as noise are present, these will most likely also be amplified. This is a drawback if applied on real data, and the effect of noise should be further investigated.

A plus is that the filter time constants that regained the ellipse shape were quite easy to find, and the same filter constant showed equal results when applied to a different case.

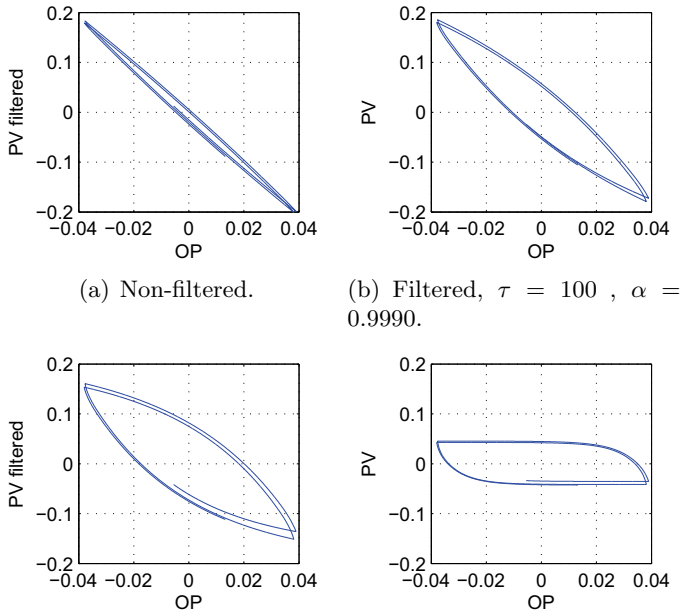

(a) Non-filtered.

(b) Filtered, $\tau = 100$, $\alpha = 0.9990$.

(c) Filtered, $\tau = 50$, $\alpha = 0.9980$.

(d) Filtered, $\tau = 10$, $\alpha = 0.9901$.

Figure 7.2: PV-OP plots with non-filtered and high-pass filtered PV data, ideal integrating process

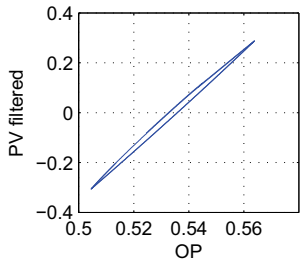

(a) Non-filtered.

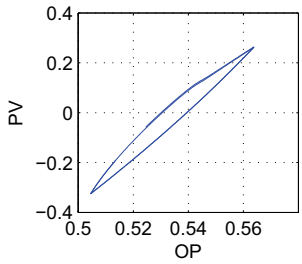

(b) Filtered, $\tau = 100$, $\alpha = 0.9990$.

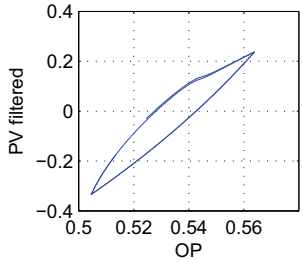

(c) Filtered, $\tau = 50$, $\alpha = 0.9980$.

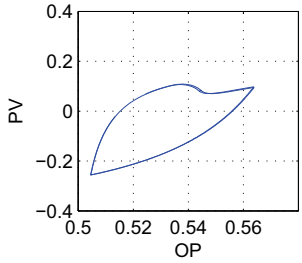

(d) Filtered, $\tau = 10$, $\alpha = 0.9901$.

Figure 7.3: PV-OP plots with non-filtered and high-pass filtered PV data, level process from production process model with constant input

Chapter 8

Conclusion and future work

8.1 Conclusion

From simulations of a production plant model, some results on how stiction affects neighboring process components was obtained. Stiction in control valves in the first stage separator affected downstream components in the plant model such as the compressor. Stiction was easy to detect and quantify from PV and OP data in the pressure process of the separator if there were no external disturbances. In the level process of the separator, there was more difficult to detect stiction from PV and OP data only.

If disturbances from slugs in the inlet stream arose, MV data had to be available to confirm the presence of stiction. Oscillations from inlet slug flow was found to be larger than stiction induced oscillations. The inlet slug flow should thus be controlled before any effort is made to remove the stiction induced oscillations.

An algorithm that detects stiction from routine operating data was proposed. The algorithm correctly detected stiction in data from an ideal non-integrating process. When applied to data from the production plant model, the algorithm concluded correct for the separator pressure process. With inlet slug flow applied, high stiction had to be present for the algorithm to conclude correct. For the separator level process, the conclusions were more uncertain.

The correctness of the algorithm when applied on real data from a offshore production plant was difficult to assess. The real case data did however, show the ability of the algorithms to cope with varying sample time and addressed its problem of coping with noise. The algorithm needs to solve the problem of noise before it can be installed in a Siemens application.

From the reported problems of detecting stiction from OP-PV data, two new ideas for stiction detection were suggested. Both ideas regain the ellipse characteristic for stiction and the results are promising, especially the idea that exploits high-pass filtering. Both the ideas need to be further studied if they are to be part of a stiction detection algorithm.

8.2 Future work

- Improve the proposed algorithm to cope with integrating processes, noise and large disturbances.
- Test the purposed algorithm on more real case sets from industry.
- Test the two new ideas on more complex data sets.
- Investigate the possibility of quantifying stiction from the two new ideas.

References

M. A. A. S. Choudhury, N.F. Thornhill, and S.L. Shah. Modelling valve stiction. *Control Engineering Practice*, 12:641–658, 2005.

M. A. A. S. Choudhury, S.L. Shah, N.F. Thornhill, and D. S. Shook. Automatic detection and quantification of stiction in control valves. *Control Engineering Practice*, 14 (12):1395–1412, 2006.

M. A. A. S. Choudhury, S. L. Shan, and N. F. Thornhill. *Diagnosis of Process Nonlinearities and Valve Stiction*. Springer, 2008.

L. Desborough and R. Miller. Increasing customer value of industrial control performance monitoring - honeywell's experience. *AIChE Symposium Series*, 98:169–189, 2002.

O. Egeland and J. T. Gravdahl. *Modeling and Simulation for Automatic Control*. Marine Cybernetics, 2003.

Fisher. *Control Valve Handbook*. Emerson Process Managment, 2005.

T. Hägglund. A control-loop performance monitor. *Control Engineering Practice*, 3:1543.1551, 1995.

T. J. Harris. Assessment of control loop performance. *Canadian Journal of Chemical Engineering*, 67:856–861, 1989.

P. Q. He, J Wang, M. Pottmann, and S. J. Qin. A curve fitting method for detecting valve stiction in oscillating control loops. *Ind. Eng. Chem.*, 46: 4549–4560, 2007.

A. Horch. A simple method for detection of stiction in control valves. *Control Engineering Practice*, 7:112–1231, 1999.

A. Horch. *Condition Monitoring of Control Loops*. PhD thesis, Dept. of Signals, Sensors and Systems, Royal Institute of Technology, Stockholm, Sweden, 2000.

A. Horch. *Process Control Performance Assessment*, chapter 7: Benchmarking Control Loops with Oscillations and Stiction, pages 227–257. Springer, 2007.

M. Hovd. Mail correspondence, May 2009.

M. Jelali. An overview of control performance assessment technology and industrial applications. *Control Engineering Practice*, 14 (5):441–466, 2006.

M. Kano, H. Maruta, H. Kugemoto, and K. Shimizu. Practical model and detection algorithm for valve stiction. *IFAC Symp. on Dyn. and Control of Proc. Syst. (DYCOPS)*, Paper no 54, 2004.

A. Kayihan and F. J. Doyle. Friction compensation for a process control valve. *Control Engineering Practice*, 8(7):799 – 812, 2000.

H. K. Khalil. *Nonlinear Systems*. Pretince Hall, 2002.

A. Kvam. Control performance monitoring - a review. Technical report, Department og Engineering Cybernetics, NTNU, 2008.

Ø. K. Kylling. Modelling and control of an offshore oil and gas plant. Technical report, Department og Engineering Cybernetics, NTNU, 2008.

A. W. Ordys, D. Uduehi, and M. A. Johnson, editors. *Process Control Performance Assessment*. Springer, 2007.

R. Rengaswamy, T. Hägglund, and V. Venkatasubramanian. A qualitative shape analysis formalism for monitoring control loop performance. *Engineering Applications of Artificial Intelligence*, 14:23–33, 2001.

M. Rossi and C. Scali. Automatic detection of stiction in actuators: A technique to reduce the number of incertain cases. *IFAC- Dycops-7th International Conference, Cambridge (USA)*, paper no 157, 2004.

T.I. Salsbury and A. Singhal. A new approach for arma pole estimation using higher-order crossings. *Proceedings of the 2005 American Control Conference, 2005.*, pages 4458–4463 vol. 7, June 2005.

A. Singhal and T. I. Salsbury. A simple method for detecting valve stiction in oscillating control loops. *Journal of Process Control*, 15 (4):371–382, 2005.

A. Stenman, F. Gustafsson, and K. Forsman. A segmentation-based method for detection of stiction in control valves. *International Journal of Adaptive Control and Signal Processing*, 17(7-9):625–634, 2003.

E. Storkaas, S. Skogestad, and Godhavn. J. M. A simple dynamic model for control design and analysis of severe slugging. *Multiphase03, San Remo, Italy*, 2003.

N. F. Thornhill. Finding the source of nonlinearity in a process with plant-wide oscillation. *Control Systems Technology, IEEE Transactions on*, 13 (3):434–443, 2005.

N. F. Thornhill and T. Hägglund. Detection and diagnosis of oscillation in control loops. *Control Engineering Practice*, 5 (10):1343–1354, 1997.

H. Torpe and F. Dessen. Anbefalinger sluggkontrol og generell regulering, internrapport, siemens, 2008.

Y. Yamashita. An automatic method for detection of valve stiction in process control loops. *Control Engineering Practice*, 14(5):503–510, 2006.

Appendix A

Simulation parameters

Table A.1: Physical parameters for production process model

Symbol	Value	Denomination
A_c	0.00956	[m^2]
ρ_{oilL}	659	[Kg/m^3]
ρ_{metL}	422	[Kg/m^3]
c_{01}	453.43	[m/s]
F_c	1250	[N]
F_v	612	[N]
k	52500	[N/m]
L_c	1.8	[m]
M_v	1.36	[kg]
p_{metV}	261	[bar]
R	8.31	[J/(K mol)]
V_{in}	0.6	[m^3]
V_{out}	0.6	[m^3]
T_c	302.95	[K]
T_{sep}	308.15	[K]
V_{sep2}	100.07	[m^3]
W_{met}	16	[g/mol]
W_{oil}	86	[g/mol]

For the control pressure valves (VPCS1 and VPCS2), the difference between the pressure set point and the operating pressure of the connected compressor is the main contribution for Δp. An additional pressure difference added to compensate for the pressure loss in the scrubber and gas cooler. The mass flows are the designed mass flows for the compressors converted into mole flow.

The designed pressure drop across the level control valve (VLCS1) of separator 1 is simply the difference in set point pressure. For the level control

Table A.2: Valve constants for production process model

Symbol	Value	Denomination	
VRVC2	–	–	0.020
VARVC3	–	–	0.025
VLCS1	9500	24 E^5	6.1
VLCS2	9500	12 E^5	8.7
VPCS1	4750	0.3 E^5	27.4
VPCS2	670	0.3E^5 3.8	

valve (VLCS2) of separator 2, the pressure drop is the difference in set point pressure and atmospheric pressure. The mass flows are the maximum flows for the inlet cases with a margin added.

Appendix B

Additional results

B.1 Additional results from simulation of production plant model

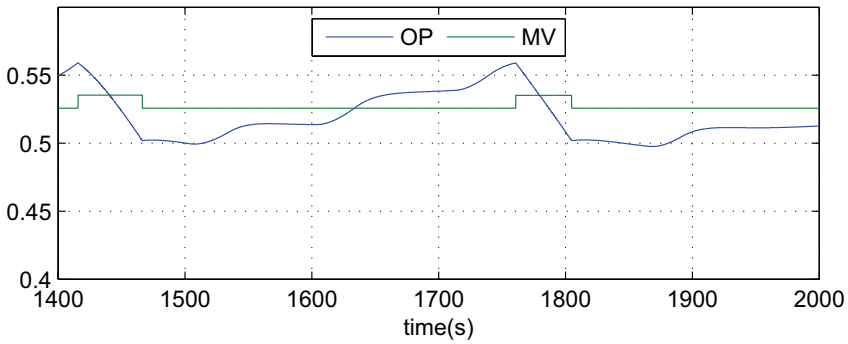

(a) Volume control valve, normal stiction.

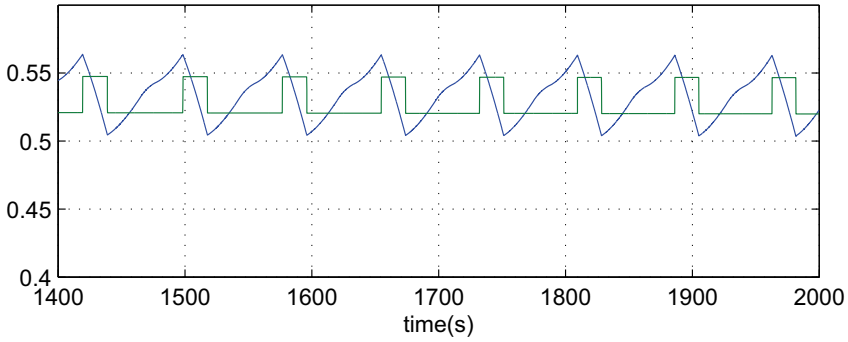

(b) Volume control valve, high stiction.

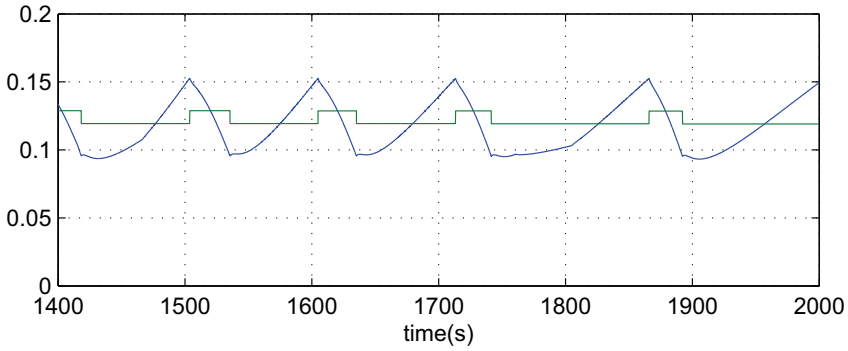

(c) Pressure control valve, normal stiction.

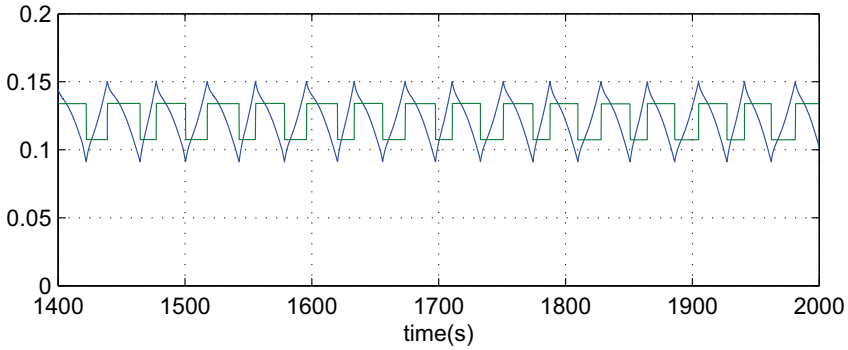

(d) Pressure control valve, normal stiction.

Figure B.1: Time plots of MV and OP data, constant methane fraction

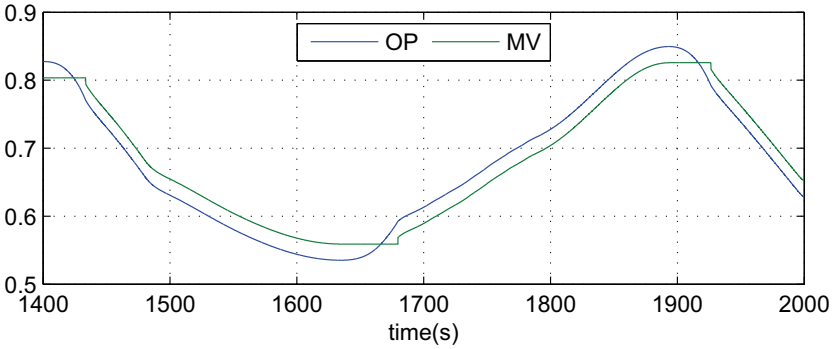

(a) Volume control valve, normal stiction.

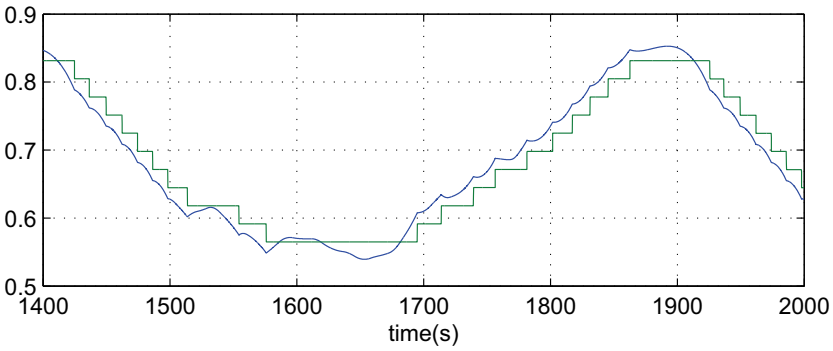

(b) Volume control valve, high stiction.

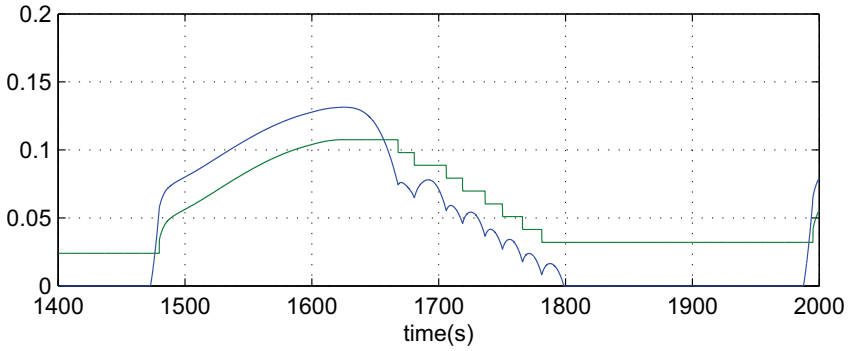

(c) Pressure control valve, normal stiction.

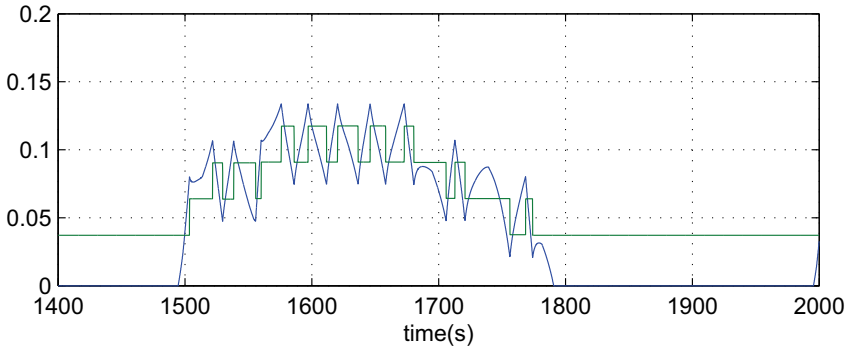

(d) Pressure control valve, normal stiction.

Figure B.2: Time plots of MV and OP data, sinusoidal methane fraction case of simulation of production process model

B.2 Additional results from testing of algorithm

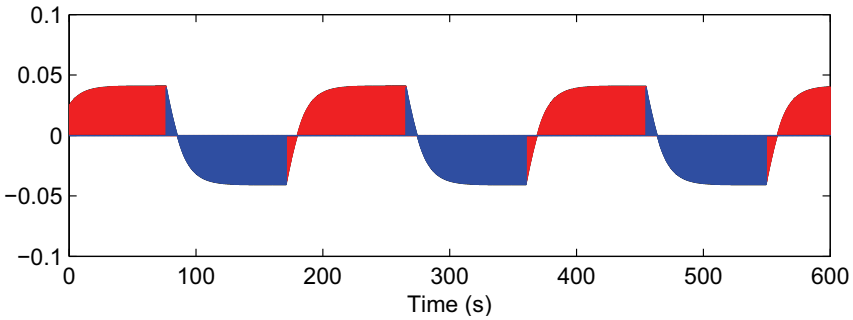

(a) Algorithm applied on data from a PI controlled first order process with high stiction and halved controller gain, $\bar{R} = 18.40 \pm 0.7$

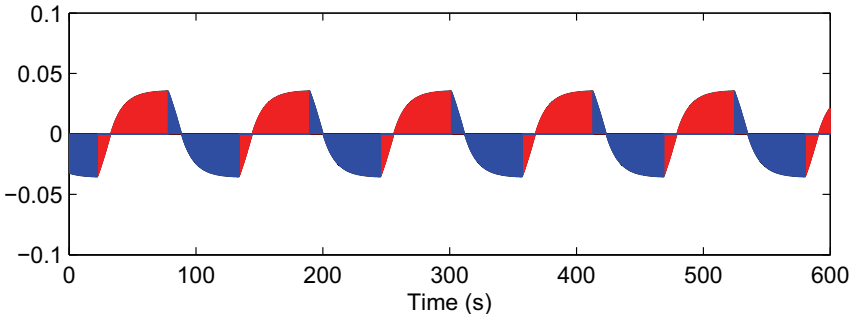

(b) Algorithm applied on data from a PI controlled first order process with normal stiction, $\bar{R} = 6.40 \pm 0.80$

Figure B.3: Algorithm test on ideal data, decreased stiction and controller gain

B.3 Additional results from testing of new ideas

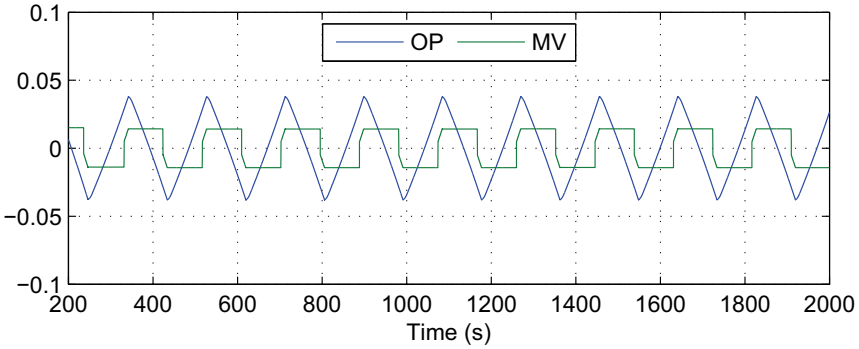

Figure B.4: Time plots of MV and OP data, ideal integrating process